
BAYESIAN INFERENCE FOR DISCRETE MARKOV RANDOM FIELDS THROUGH COORDINATE RESCALING

Giuseppe Arena

Department of Psychology
University of Amsterdam
g.arena@uva.nl

Maarten Marsman

Department of Psychology
University of Amsterdam
m.marsman@uva.nl

This manuscript has not yet been peer-reviewed.

Corresponding author: Giuseppe Arena[✉], Department of Psychology, University of Amsterdam – Nieuwe Achtergracht 129-B, PO Box 15906, 1001 NK Amsterdam, The Netherlands – E-mail: g.arena@uva.nl.

Keywords Markov random fields · undirected graphical models · intractable posterior · posterior inference

ABSTRACT

Discrete Markov random fields (MRFs) represent a class of undirected graphical models that capture complex conditional dependencies between discrete variables. Conducting exact posterior inference in these models is computationally challenging due to the intractable partition function, which depends on the model parameters and sums over all possible state configurations in the system. As a result, using the exact likelihood function is infeasible and existing methods, such as Double Metropolis-Hastings or pseudo-likelihood approximations, either scale poorly to large systems or underestimate the variability of the target posterior distribution. To address both computational burden and efficiency loss, we propose a new class of coordinate-rescaling sampling methods, which map the model parameters from the pseudo-likelihood space to the target posterior, preserving computational efficiency while improving posterior inference. Finally, in simulation studies, we compare the proposed method to existing approaches and illustrate that coordinate-rescaling sampling provides more accurate estimates of posterior variability, offering a scalable and robust solution for Bayesian inference in discrete MRFs.

1 Introduction

Markov Random Fields (MRFs) are a class of undirected graphical models that represent conditional dependencies between variables through the structure of an undirected Markov graph (Besag, 1974; Kindermann and Snell, 1980). In this graph (or “network”), nodes represent the random variables. For instance, in functional magnetic resonance imaging, they may represent individual’s brain responses; in genetics, they may reflect gene or protein expression levels, and, in psychology, they may illustrate mental health symptoms. The edges between the variables encode conditional dependencies, such that after considering the remaining variables, the absence of an edge between two variables implies that they are independent from each other. MRFs represent conditional dependencies using pairwise interactions, with the network structure embedded in the partial association parameters of the model. Common example of MRFs include, the Ising model for network of binary variables (Ising, 1925), the ordinal MRF for networks of variables measured on discrete ordered values (Marsman et al., 2025), and the Gaussian graphical models for networks of continuous variables (Lauritzen, 1996).

In this paper, we focus on the Bayesian analysis of Markov Random Fields for discrete variables. This approach is motivated by the fact that the posterior distribution of discrete MRFs is doubly intractable (Murray et al., 2006). Both the likelihood and the posterior normalizing constant depend on the partition function which is computationally expensive to calculate. In contrast, Gaussian graphical models provide a fully tractable posterior distribution, while intractability arises when integrating the graph structure into the Bayesian framework, which leads to an intractable posterior where the normalizing constant of the G-Wishart prior must be approximated for each proposed graph (Lenkoski and Dobra, 2011; Mohammadi and Wit, 2015). The contribution of this paper is to present a computationally efficient method for addressing the double intractability problem of the posterior distribution and conducting Bayesian inference in discrete Markov Random Fields.

The computational complexity in discrete MRFs lies in the normalizing constant of the likelihood. For a parameter vector $\boldsymbol{\theta}$, the likelihood

$$f(\mathbf{X}; \boldsymbol{\theta}) = \frac{1}{Z(\boldsymbol{\theta})} \exp \{-E(\mathbf{X}; \boldsymbol{\theta})\}$$

requires the computation of the normalizing constant (or “partition function”)

$$Z(\boldsymbol{\theta}) = \sum_{\mathbf{X}' \in \mathcal{X}} \exp \{-E(\mathbf{X}'; \boldsymbol{\theta})\},$$

that is the sum of the energy value over all the possible state configurations in the system. Calculating the partition function $Z(\boldsymbol{\theta})$ at each iteration of the estimation process is computationally expensive, especially in large systems, as it requires evaluating the model across all possible state configurations. This complexity has a significant impact on the efficiency of model parameter estimation. The size

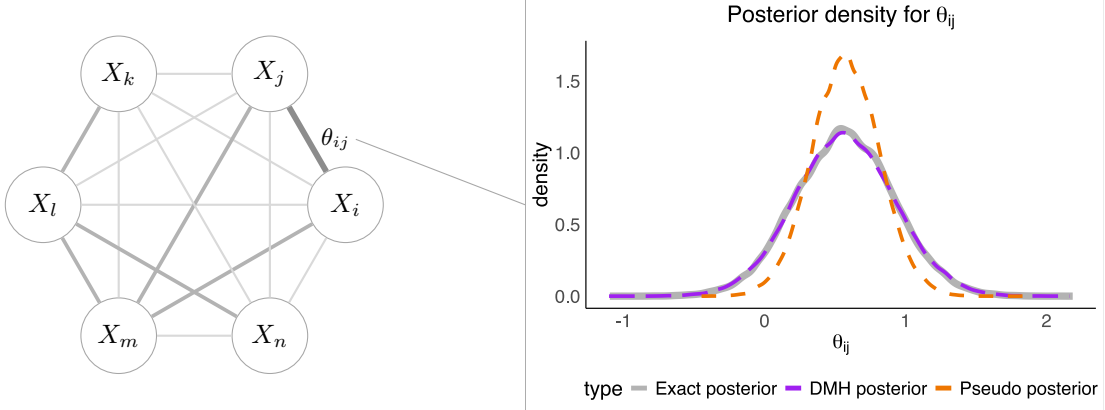


Figure 1: (Left) Example of small-scale system consisting of six random variables. The grayscale intensity and edge thickness are proportional to the posterior absolute mode of the pairwise associations: stronger associations (in absolute value) correspond to darker and thicker edges. The parameter θ_{ij} quantifies the conditional dependence between the variables X_i and X_j given the remaining variables in the system. (Right) Posterior density of the pairwise association θ_{ij} : the gray solid line represents the posterior results from the full likelihood (Exact posterior), the orange dashed line the posterior based on pseudo-likelihood function (Pseudo posterior) and the dashed purple line the posterior based on the Double Metropolis-Hastings algorithm (DMH posterior).

of the partition function grows exponentially with the number of nodes and possible states in the network, leading to a larger number of parameters to estimate. For instance, with 10 random binary variables (e.g. presence / absence of a symptom), the number of states is $2^{10} = 1,024$, while for 10 variables measured on four categories, it becomes $4^{10} = 1,048,576$. In a Bayesian framework, conducting Bayesian inference on the network parameters introduces additional significant challenges due to the double-intractability of the posterior distribution. After assuming a prior distribution $\pi(\boldsymbol{\theta})$ over the model parameters $\boldsymbol{\theta}$, the corresponding posterior distribution of the parameters is defined as

$$\pi(\boldsymbol{\theta} \mid \mathbf{X}) = \frac{f(\mathbf{X}; \boldsymbol{\theta})\pi(\boldsymbol{\theta})}{f(\mathbf{X})},$$

where the complexity of the partition function is combined with that of the marginal likelihood

$$f(\mathbf{X}) = \int_{\mathbb{R}^{|\boldsymbol{\theta}|}} f(\mathbf{X}; \boldsymbol{\theta})\pi(\boldsymbol{\theta}) d\boldsymbol{\theta}.$$

Several strategies have been proposed to address double intractability in discrete MRFs. One prominent approach is the Double Metropolis-Hastings (DMH) of [Park and Haran \(2018\)](#), which approximates the intractable ratio between partition functions with auxiliary MCMC approximations. As illustrated in Figure 1, DMH can produce accurate posterior estimates, but at a significant computational cost (runtime ≈ 9 minutes¹ for the example in Figure 1), limiting the scalability of the approach to large systems. An alternative class of methods relies on the pseudo-likelihood

¹Time performance based on C++-coded functions, run on a Macbook Air (2024) with Apple M3 chip, 8-CPUs and 16Gb RAM.

function (Lindsay, 1988), which approximates the full likelihood function with a product of conditional distributions for each node given the remaining nodes, avoiding the need for the partition function (Yang et al., 2014; Florez et al., 2025). Pseudo-likelihood formulations have gained popularity in MRFs, as they provide a feasible alternative to likelihood functions that can be computationally expensive (Pensar et al., 2017; Marsman et al., 2022; Mohammadi et al., 2025). Although often overlooked due to its less efficient performance in other models, such as Exponential Random Graph models (ERGMs; van Duijn et al., 2009; Schmid and Desmarais, 2017) or Gaussian Graphical models (GGMs; Huth et al., 2025), pseudo-likelihood estimation is computationally extremely fast (runtime ≈ 14 seconds¹ for the example in Figure 1) and provides unbiased parameter estimates for discrete MRFs (Keetelaar et al., 2024). However, as illustrated in Figure 1, the variability of the posterior distribution may result underestimated (Miller, 2021). To address such efficiency loss, Bouranis et al. (2017) proposed a post hoc rescaling of the pseudo posterior to correct for its variance in the context of ERGMs. While their method is tailored to ERGMs, the idea can be extended to discrete MRFs, where the pseudo posterior variability is underestimated although without the location bias observed in ERGMs. On the other hand, their post hoc calibration step may be computationally expensive when posterior estimates must be recomputed anytime that the data changes and in large systems where an accurate estimation of the target covariance is required. Therefore, the central challenge is to develop sampling methods that preserve the computational scalability of the pseudo-likelihood (or alternative composite likelihood functions), while providing robust posterior inference, and avoiding the efficiency loss associated with the pseudo-likelihood approach.

To address this challenge, we present a two-fold contribution. First, we introduce a new class of sampling techniques, the “coordinate-rescaling” methods, which address this challenge by modifying the scale of the target distribution through a linear transformation of the parameters from the pseudo-likelihood space to the target space, while preserving the Markovian properties and converging to the target distribution. This new class of sampling methods provides convergence to the target distribution (as illustrated in Figure 1), scalability and computational efficiency (runtime ≈ 28 seconds¹ for the example in Figure 1). The second contribution of this work focuses on the performance comparison of the new methodology relative to existing approaches using simulation-based studies. Existing methods include post hoc calibration (Bouranis et al., 2017), DMH sampling (Park and Haran, 2018), and covariance-based adaptive proposals (Haario et al., 2001). In addition to these methods, we introduce an adaptive sampler that relies on a surrogate likelihood function, the “empirical likelihood”.

The remainder of the paper is organized as follows. In section 2, we outline the full likelihood function and the pseudo-likelihood approximation of an ordinal MRF, a subclass of discrete MRFs characterized by variables measured on an ordered scale. Although our focus is on ordinal variables, the methodology presented can be readily adapted to any discrete MRF. In section 3, we introduce

the “coordinate-rescaling” methods, explaining their theoretical foundation and how rescaling the target posterior improves posterior density exploration. In section 4, we present an overview of existing approaches and introduce the empirical likelihood function. In section 5, we compare the new methodology with existing approaches using simulation studies to highlight strengths and limitations. Finally, in section 6, we discuss the results, highlight the shortcomings and advantages of the novel methodology compared to the existing approaches, and delineate directions for future work.

2 Discrete Markov Random Fields

Building upon the MRF framework, a discrete Markov random field represents the conditional dependencies arising between random variables that assume a finite set of values (or categories). As a concrete example, let $\mathbf{X} = (\mathbf{X}_1, \dots, \mathbf{X}_n)$ denote the observed data for n samples on p ordinal variables, where $\mathbf{X}_\nu = (X_{\nu 1}, \dots, X_{\nu p})$, represents the p -variate vector of observed values for the ν -th sample (with $\nu = 1, \dots, n$), and each variable in the system assumes $m + 1$ categories. The full likelihood function of a discrete Markov random field for a sample of n observations can be written as the product of the probability density function f for each observed sample, that is,

$$f(\mathbf{X}_1, \dots, \mathbf{X}_n; \boldsymbol{\theta}) = \prod_{\nu=1}^n f(\mathbf{X}_\nu; \boldsymbol{\theta}) = \frac{1}{Z(\boldsymbol{\theta})^n} \exp \{ \mathbf{s}(\mathbf{X})^\top \boldsymbol{\theta} \} \quad (1)$$

where: (i) $\boldsymbol{\theta} \in \mathbb{R}^{|\boldsymbol{\theta}|}$ is the set of model parameters including the marginal effects of the p random variables and the pairwise associations between variables, (ii) $\mathbf{X}_\nu \in \mathcal{X}$ is the value of the p variables observed in the ν -th sample, which is a realization from the set of possible configurations $\mathcal{X} = \{0, 1, \dots, m\}^p$. When considering discrete variables with values following the order $\{0 < 1 < \dots < m\}$, the state space can be modeled as an ordinal Markov random field (OMRF; [Marsman et al., 2025](#)). Thus, we can express the sum of the energy $E(\cdot)$ over all observed states \mathbf{X} in a compact notation as

$$-\sum_{\nu=1}^n E(\mathbf{X}_\nu; \boldsymbol{\theta}) = \sum_{i=1}^p \sum_{h=1}^m \mu_{ih} \left(\sum_{v=1}^n \mathcal{I}(X_{\nu i} = h) \right) + \sum_{i < j} \theta_{ij} \left(\sum_{v=1}^n X_{\nu i} X_{\nu j} \right) = \mathbf{s}(\mathbf{X})^\top \boldsymbol{\theta},$$

that is, the inner product between the vector of sufficient statistics $\mathbf{s}(\mathbf{X})$ calculated from the observed samples and the vector of model parameters $\boldsymbol{\theta}$. Sufficient statistics consist of two types: $p \times m$ statistics that measure the observed frequency of m ordered categories for each variable (excluding the baseline category) and $p \times (p - 1)/2$ statistics that quantify the summed cross products between pairs of variables. The corresponding parameters are the “threshold” parameters, μ_{ih} , which quantify the tendency of variable i to take on a specific non-baseline category h , and the “interaction” parameters, θ_{ij} , which capture the pairwise conditional dependency between variables i and j . When the p

variables are measured on a binary scale, the OMRF reduces to the well-known Ising model, a mathematical model of ferromagnetism introduced by [Ising \(1925\)](#).

The likelihood function in (1) is also referred to as full likelihood because it is a joint likelihood that accounts for all pairwise dependencies between the nodes in the network, capturing the global properties of an OMRF. However, as discussed in the introduction section, performing Bayesian inference using the full likelihood is computationally expansive because of the double-intractable posterior distribution. To address this problem, we can use a composite likelihood approach. In the next section, we introduce the pseudo-likelihood function, a specific composite likelihood that approximates the full likelihood.

2.1 The pseudo-likelihood function: composite likelihood for ordinal Markov Random Fields

Composite likelihood functions are often implemented when the full likelihood is difficult to define or computationally complicated to optimize ([Lindsay, 1988](#)). The idea behind composite likelihood functions is to approximate a joint probability of random variables by combining likelihood components that are derived from a subset of the data or by simplified dependency structures. The pseudo-likelihood is a specific case of composite likelihood, which defines a likelihood function as the product of conditional likelihoods for a subset or all of the variables, with the aim of simplifying the computation and making the estimation feasible when the full likelihood function is intractable ([Besag, 1986](#)).

Let $\mathbf{X} = (X_1, \dots, X_p)$ denote p random variables, as defined for the full likelihood, and let $\mathbf{X}_{(-i)}$ be the set of nodes excluding node X_i . The full likelihood for a single observation \mathbf{X} can be written as the product of conditional distributions of each node \mathbf{X}_i given the remaining nodes $\mathbf{X}_{(-i)}$, that is,

$$\tilde{f}(\mathbf{X}; \boldsymbol{\theta}) = \prod_{i=1}^p f(X_i | \mathbf{X}_{(-i)}, \boldsymbol{\theta}) \quad (2)$$

The pseudo-likelihood function for a sample of size n is then the product of the pseudo-likelihood for each observation in the sample,

$$\tilde{f}(\mathbf{X}_1, \dots, \mathbf{X}_n; \boldsymbol{\theta}) = \prod_{\nu=1}^n \tilde{f}(\mathbf{X}_\nu; \boldsymbol{\theta}) = \frac{1}{\tilde{Z}(\mathbf{X}_1, \dots, \mathbf{X}_n, \boldsymbol{\theta})} \exp \{ \tilde{\mathbf{s}}(\mathbf{X})^\top \boldsymbol{\theta} \}, \quad (3)$$

where, the sufficient statistics $\tilde{\mathbf{s}}(\mathbf{X})$ are similar to those of the full likelihood, with the key difference that pairwise cross products are doubled. The normalizing constant is written as

$$\tilde{Z}(\mathbf{X}_1, \dots, \mathbf{X}_n, \boldsymbol{\theta}) = \prod_{\nu=1}^n \tilde{Z}(\mathbf{X}_\nu, \boldsymbol{\theta}) = \prod_{\nu=1}^n \prod_{i=1}^p \left[1 + \sum_{h=1}^m \exp \left(\mu_{ih} + h \sum_{j \neq i} \theta_{ij} X_{\nu j} \right) \right],$$

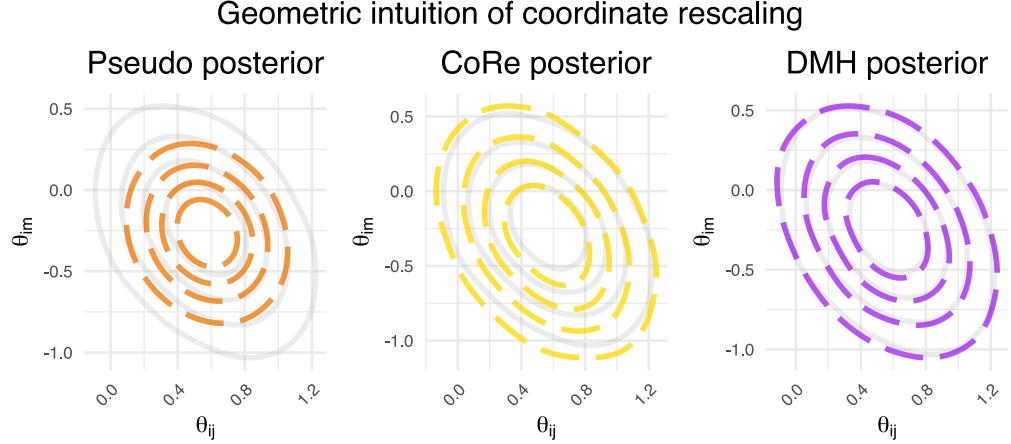


Figure 2: Contour lines representing the posterior distribution of two pairwise association parameters, θ_{ij} and θ_{im} . (Left) The pseudo posterior distribution (orange dashed contours) and the exact posterior (gray solid contours). (Center) The CoRe posterior distribution (gold dashed contours) and the exact posterior (gray solid contours). (Right) The DMH posterior distribution (purple dashed contours) and the exact posterior (gray solid contours).

that is distinct for each observation and computationally tractable.

The pseudo-likelihood is widely used because it easily scales up to high-dimensional graphs, remaining a tractable function, with maximum pseudo-likelihood estimates consistent (Arnold and Strauss, 1991; Geys et al., 1997) and unbiased with respect to the maximum likelihood estimates (Keetelaar et al., 2024). However, as already outlined earlier, the pseudo-likelihood may not accurately capture the global dependencies between variables, which can affect the efficiency of the posterior distributions (Miller, 2021).

In the context of OMRFs, the quality of posterior inference substantially depends on balancing computational tractability with statistical efficiency. The use of the full likelihood is feasible only when the variables in the network are binary (as in the Ising model) and the number of nodes is sufficiently small to evaluate the partition function within a reasonable time. However, in most practical settings, the pseudo-likelihood provides a valid alternative to approximate the posterior distribution of the model parameters. In the next section, we address the trade-off between computational feasibility and statistical efficiency by introducing a novel methodology that maintains the scalability of the pseudo-likelihood while ensuring robust posterior inference.

3 Approximate Posterior Inference via Coordinate Rescaling

Sampling from the exact posterior of an OMRF requires the calculation of the partition function $Z(\boldsymbol{\theta})$ at each iteration. In a standard Metropolis-Hastings algorithm, let $q(\boldsymbol{\theta}'|\boldsymbol{\theta})$ denote the proposal distribution for the parameter $\boldsymbol{\theta}$, which generates a candidate move from $\boldsymbol{\theta}$ to $\boldsymbol{\theta}'$. The move is

accepted with probability

$$\alpha(\boldsymbol{\theta}, \boldsymbol{\theta}') = \min \left\{ 1, \frac{\pi(\boldsymbol{\theta}'|\mathbf{X})q(\boldsymbol{\theta}|\boldsymbol{\theta}')}{\pi(\boldsymbol{\theta}|\mathbf{X})q(\boldsymbol{\theta}'|\boldsymbol{\theta})} \right\} = \min \left\{ 1, \frac{f(\mathbf{X}; \boldsymbol{\theta}')\pi(\boldsymbol{\theta}')q(\boldsymbol{\theta}|\boldsymbol{\theta}')}{f(\mathbf{X}; \boldsymbol{\theta})\pi(\boldsymbol{\theta})q(\boldsymbol{\theta}'|\boldsymbol{\theta})} \right\},$$

where $\frac{f(\mathbf{X}; \boldsymbol{\theta}')}{f(\mathbf{X}; \boldsymbol{\theta})}$ includes the intractable ratio of partition functions $Z(\boldsymbol{\theta})/Z(\boldsymbol{\theta}')$. A wide range of algorithms have been proposed to overcome the complexity of the partition function. For instance, the DMH algorithm (Murray et al., 2006; Park and Haran, 2018) takes advantage of Monte Carlo estimation and auxiliary variable schemes, introducing an inner Metropolis step to generate auxiliary data $\mathbf{Y} \sim p(\cdot|\boldsymbol{\theta}')$ and replace the ratio between partition function. Hence, in the DMH algorithm, a candidate move from $\boldsymbol{\theta}$ to $\boldsymbol{\theta}'$ becomes,

$$\begin{aligned} \alpha(\boldsymbol{\theta}, \boldsymbol{\theta}') &= \min \left\{ 1, \frac{f(\mathbf{X}; \boldsymbol{\theta}')f(\mathbf{Y}; \boldsymbol{\theta})\pi(\boldsymbol{\theta}')q(\boldsymbol{\theta}|\boldsymbol{\theta}')}{f(\mathbf{X}; \boldsymbol{\theta})f(\mathbf{Y}; \boldsymbol{\theta}')\pi(\boldsymbol{\theta})q(\boldsymbol{\theta}'|\boldsymbol{\theta})} \right\} \\ &= \min \left\{ 1, \frac{\exp \{ \mathbf{s}(\mathbf{X})^\top \boldsymbol{\theta}' \} Z(\boldsymbol{\theta}) \exp \{ \mathbf{s}(\mathbf{Y})^\top \boldsymbol{\theta} \} Z(\boldsymbol{\theta}') \pi(\boldsymbol{\theta}')q(\boldsymbol{\theta}|\boldsymbol{\theta}')}{\exp \{ \mathbf{s}(\mathbf{X})^\top \boldsymbol{\theta} \} Z(\boldsymbol{\theta}') \exp \{ \mathbf{s}(\mathbf{Y})^\top \boldsymbol{\theta}' \} Z(\boldsymbol{\theta}) \pi(\boldsymbol{\theta})q(\boldsymbol{\theta}'|\boldsymbol{\theta})} \right\}, \end{aligned}$$

where the partition function cancels out, simplifying the determination of the acceptance ratio. However, these methods can be computationally intensive due to the nested sampling scheme, the need for an exact or approximate sampler, and potential issues with poor mixing caused by noise in the auxiliary simulations \mathbf{Y} . An alternative line of work relies on pseudo-likelihood-based posterior inference. Although in such a case the partition function becomes tractable, the resulting posterior distributions tend to overly concentrate around the posterior mode, underestimating the posterior uncertainty (as illustrated in Figure 1).

We introduce here a new sampling strategy that combines the computational efficiency of the pseudo-likelihood with robust posterior inference. We build on the idea of post hoc calibration of pseudo posterior samples introduced by Bouranis et al. (2017) and define a new sampling scheme for discrete MRFs. We refer to this method as “coordinate rescaling” (in short, “CoRe”), which offers a principled approach to sample from the approximate exact posterior via geometrically reweighting the pseudo posterior. The method applies a linear transformation to the parameter space during the sampling process, which results in the rotation of the posterior contours. This rotation is based on an appropriate choice of the rescaling matrix, which provides a robust approximation of the variability and correlation structure of the target posterior. In the following paragraphs, we discuss the details of two versions of the new sampling scheme: the standard CoRe sampler, where the rescaling matrix is precomputed before sampling, and its adaptive version, the “AdaCoRe” sampler, where the same matrix is iteratively estimated during the burn-in stage.

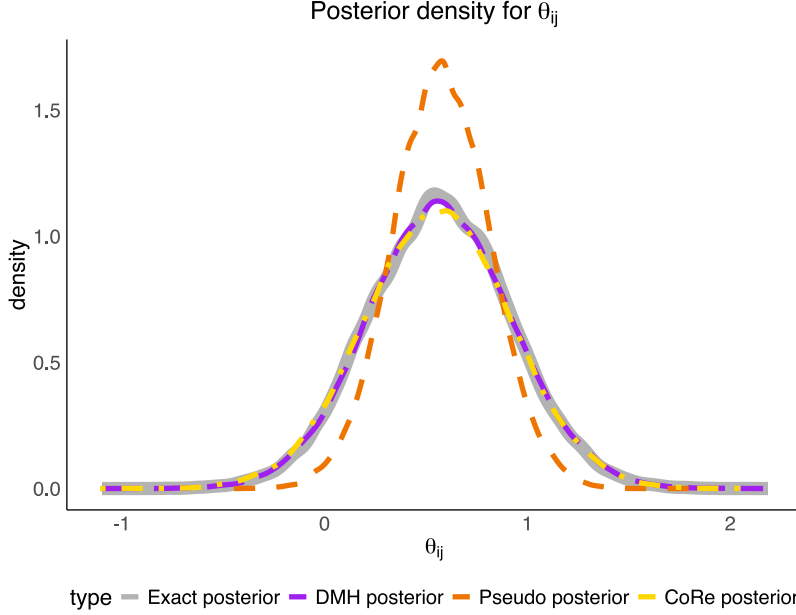


Figure 3: Posterior density of the pairwise association θ_{ij} : the gray solid line represents the posterior results from the full likelihood (Exact posterior), the orange dashed line the posterior based on pseudo-likelihood function (Pseudo posterior), the dashed purple line the posterior based on the Double Metropolis-Hastings algorithm (DMH posterior) and the dotdashed yellow line the posterior based on the CoRe sampling (CoRe posterior).

Algorithm 1 Coordinate Rescaling (CoRe) sampling scheme

Input: β and θ at the s -th iteration, the observed data $\mathbf{X} = (\mathbf{X}_1, \dots, \mathbf{X}_n)$, the inverse rescaling matrix \mathbf{A}^{-1} , and θ^* .

Propose $\beta' \sim q(\cdot | \beta)$.

Calculate $\theta' = \mathbf{A}^{-1}(\beta' - \theta^*) + \theta^*$.

Accept $\beta_{s+1} = \beta'$ and $\theta_{s+1} = \theta'$ with probability

$$\alpha(\beta, \beta') = \min \left\{ 1, \frac{\tilde{f}(\mathbf{X}; \theta') \pi(\theta') q(\beta | \beta')}{\tilde{f}(\mathbf{X}; \theta) \pi(\theta) q(\beta' | \beta)} \right\},$$

otherwise reject and set $\beta_{s+1} = \beta$ and $\theta_{s+1} = \theta$.

3.1 The CoRe sampler

Let θ denote the parameters on the pseudo posterior scale, β the parameters on the transformed scale, we define the linear transformation

$$\beta = \mathbf{A}(\theta - \theta^*) + \theta^*,$$

where θ^* can be a maximum a posteriori estimate (MAP) or a maximum pseudo-likelihood estimate (MPLE) for θ , \mathbf{A} is the rescaling matrix that performs a rotation of the parameters from the pseudo posterior scale to the transformed scale. The linear transformation above aligns with that proposed by Bouranis et al. (2017) in the post hoc calibration of pseudo-likelihood-based posterior draws, with

the difference that our method embeds the transformation within the sampling scheme and does not require the iterative estimation of $\boldsymbol{\theta}^*$ since the MPLEs for discrete MRFs are unbiased (Keetelaar et al., 2024). The CoRe approach defines a posterior distribution $\pi(\boldsymbol{\beta}|\mathbf{X})$ on the transformed parameters $\boldsymbol{\beta}$. We find the analytical definition of this distribution by operating the change of variables $\boldsymbol{\theta} \rightarrow \boldsymbol{\beta}$, that is,

$$\pi(\boldsymbol{\beta}|\mathbf{X}) = \pi(\boldsymbol{\theta}(\boldsymbol{\beta})|\mathbf{X}) \left| \det \left(\frac{\partial \boldsymbol{\theta}(\boldsymbol{\beta})}{\partial \boldsymbol{\beta}} \right) \right|$$

where $\boldsymbol{\theta}(\boldsymbol{\beta}) = \mathbf{A}^{-1}(\boldsymbol{\beta} - \boldsymbol{\theta}^*) + \boldsymbol{\theta}^*$ is the inverse transformation $\boldsymbol{\beta} \rightarrow \boldsymbol{\theta}$, and $\left| \det \left(\frac{\partial \boldsymbol{\theta}(\boldsymbol{\beta})}{\partial \boldsymbol{\beta}} \right) \right| = \left| \det(\mathbf{A})^{-1} \right|$ is the Jacobian, which remains constant while sampling as the inverse of the rescaling matrix \mathbf{A} is precomputed and fixed. The sampler then targets the modified posterior $\pi(\boldsymbol{\beta}|\mathbf{X})$ and proposes a new state $\boldsymbol{\beta}'$ from a proposal distribution $q(\boldsymbol{\beta}'|\boldsymbol{\beta})$ on the $\boldsymbol{\beta}$ -scale. Finally, the acceptance ratio $\alpha(\boldsymbol{\beta}, \boldsymbol{\beta}')$ is calculated accounting for the change of variables as follows,

$$\begin{aligned} \alpha(\boldsymbol{\beta}, \boldsymbol{\beta}') &= \min \left\{ 1, \frac{\pi(\boldsymbol{\beta}'|\mathbf{X})q(\boldsymbol{\beta}|\boldsymbol{\beta}')}{\pi(\boldsymbol{\beta}|\mathbf{X})q(\boldsymbol{\beta}'|\boldsymbol{\beta})} \right\} \\ &= \min \left\{ 1, \frac{\tilde{f}(\mathbf{X}; \boldsymbol{\theta}(\boldsymbol{\beta}')) \pi(\boldsymbol{\theta}(\boldsymbol{\beta}')) \left| \det(\mathbf{A})^{-1} \right| q(\boldsymbol{\beta}|\boldsymbol{\beta}')} {\tilde{f}(\mathbf{X}; \boldsymbol{\theta}(\boldsymbol{\beta})) \pi(\boldsymbol{\theta}(\boldsymbol{\beta})) \left| \det(\mathbf{A})^{-1} \right| q(\boldsymbol{\beta}'|\boldsymbol{\beta})} \right\}. \end{aligned}$$

Although the sampling scheme rescales the target distribution of interest, it retains both the Markovian structure and the detailed balance. We provide the steps of the CoRe sampling scheme in Algorithm 1.

Figure 2 illustrates the posterior distribution of two parameters θ_{ij} and θ_{im} (from the previous example in Section 1): the pseudo posterior distribution (left) shows contours that are much more concentrated compared to the exact posterior (gray contours), the CoRe posterior (center) presents expanded contours matching the shape of the exact posterior, and, finally, the DMH posterior (right) shows contours that approach those of the exact posterior. Next to the posterior matching, CoRe sampling (and the DMH too) is able to recover the non-zero covariances between parameters, which are not captured by the pseudo-likelihood, as illustrated in Figure 2 by the rotation of the posterior contours. For a more detailed comparison, in Appendix A, we compare the posterior correlations from the CoRe posterior, the pseudo posterior and the DMH posterior over increasing sample sizes (n). The CoRe posterior correlations are unbiased but less precise, and their efficiency improves with the number of observations. For continuity, in Figure 3 we revisit the example introduced in Figure 1 and compare the behavior of the pseudo posterior, the posterior based on the DMH algorithm and the CoRe posterior. Our proposed method takes ≈ 28 seconds¹ to run one chain and provides a satisfactory overlap with the exact posterior, comparable to that achieved by the DMH algorithm, which requires a significantly longer runtime. Next to the formal definition and the

geometric intuition of the CoRe sampling, we now provide more technical details on the rescaling matrix \mathbf{A} .

3.2 The rescaling matrix \mathbf{A}

The role of the rescaling matrix \mathbf{A} is central to the CoRe sampling idea. In principle, the sampler operates with its inverse, \mathbf{A}^{-1} , however, in the remainder of this section, we discuss the definition of matrix \mathbf{A} to maintain the readability and the relationship to its components. The matrix is calculated as,

$$\mathbf{A} = \mathbf{\Gamma} \mathbf{L}^\top,$$

where:

- \mathbf{L}^\top is the upper triangular from the Cholesky decomposition of the negative posterior Hessian evaluated at $\boldsymbol{\theta}^*$, representing the inverse of the pseudo-likelihood-based posterior scale, and is calculated as

$$\mathbf{L} \mathbf{L}^\top = -(\mathbf{H} + \mathbf{H}_{\boldsymbol{\theta}}),$$

where \mathbf{H} is the Hessian matrix of the pseudo-likelihood, $\mathbf{H}_{\boldsymbol{\theta}}$ is the log-prior curvature, and both are evaluated at $\boldsymbol{\theta}^*$.

- $\mathbf{\Gamma}$ is the lower triangular from the Cholesky decomposition evaluated at $\boldsymbol{\theta}^*$ of the scale matrix that captures the variability and the correlation structure of the target posterior. In our definition, we choose the scale matrix $\mathbf{\Gamma} \mathbf{\Gamma}^\top$ to match the robust posterior covariance estimator based on the result of [Godambe \(1960\)](#), [Huber \(1967\)](#), and [White \(1980\)](#). We refer to this covariance as the “Godambe-Huber-White” posterior scale matrix (in short, “GHW”) and we calculate it as the GHW estimator corrected by the curvature of the prior distribution on $\boldsymbol{\theta}$. Let $\boldsymbol{\Sigma}_{\text{GHW}}$ denote the Godambe-Huber-White covariance estimator evaluated at $\boldsymbol{\theta}^*$,

$$\boldsymbol{\Sigma}_{\text{GHW}} = (-\mathbf{H}^{-1}) \times \mathbf{U} \times (-\mathbf{H}^{-1})$$

where $\mathbf{U} = \sum_{\nu=1}^n \mathbf{u}_\nu \mathbf{u}_\nu^\top$ is the variance of the score, defined as the sum of the outer products of the score vectors \mathbf{u}_ν for each individual. The robust posterior covariance estimator is then calculated as

$$\mathbf{\Gamma} \mathbf{\Gamma}^\top_{\text{GHW}} = (\boldsymbol{\Sigma}_{\text{GHW}}^{-1} - \mathbf{H}_{\boldsymbol{\theta}})^{-1},$$

where the estimator accounts for the log-prior curvature $\mathbf{H}_{\boldsymbol{\theta}}$.

In the standard version of the CoRe method, the inverse transformation $\boldsymbol{\theta} \rightarrow \boldsymbol{\beta}$ requires the inverse of the rescaling matrix, $\mathbf{A}^{-1} = \mathbf{L}^{-\top} \mathbf{\Gamma}^{-1}$, which is precomputed before sampling. However, in the

Algorithm 2 Inverse rescaling matrix update for iteration $s + 1$

Input: running mean $\bar{\theta}_s$ at the s -th iteration, the observed data $\mathbf{X} = (\mathbf{X}_1, \dots, \mathbf{X}_n)$ and an identity matrix \mathbf{I} of the same dimension of the parameter vector θ .
Calculate score covariance $\mathbf{U}_s = \sum_{\nu=1}^n \nabla \log \tilde{f}(\mathbf{X}_\nu; \bar{\theta}_s) \nabla \log \tilde{f}(\mathbf{X}_\nu; \bar{\theta}_s)^\top$.
Calculate model Hessian $\mathbf{H}_s = \sum_{\nu=1}^n \nabla^2 \log \tilde{f}(\mathbf{X}_\nu; \bar{\theta}_s)$.
Calculate prior Hessian $\mathbf{H}_{\theta,s} = \text{diag}(\nabla^2 \log \pi(\bar{\theta}_s))$.
Solve $\mathbf{U}_s \mathbf{Z}_s = -\mathbf{H}_s$ for \mathbf{Z}_s (i.e., $\mathbf{Z}_s := \mathbf{U}_s^{-1}(-\mathbf{H}_s)$).
Calculate robust posterior covariance estimator $\mathbf{\Gamma} \mathbf{\Gamma}^\top_{\text{GHW}} = ((-\mathbf{H}_s) \mathbf{Z}_s - \mathbf{H}_{\theta,s})^{-1}$.
Find lower triangular $\mathbf{\Gamma}_{\text{GHW}} \leftarrow \text{chol}(\mathbf{\Gamma} \mathbf{\Gamma}^\top_{\text{GHW}})$.
Solve $\mathbf{\Gamma}_{\text{GHW}} \tilde{\mathbf{\Gamma}} = \mathbf{I}$ for $\tilde{\mathbf{\Gamma}}$ (i.e., $\tilde{\mathbf{\Gamma}} := \mathbf{\Gamma}_{\text{GHW}}^{-1}$).
Calculate posterior curvature $\mathbf{L} \mathbf{L}^\top = -(\mathbf{H}_s + \mathbf{H}_{\theta,s})$.
Find upper triangular $\mathbf{L}^\top \leftarrow \text{chol}(\mathbf{L} \mathbf{L}^\top)$.
Solve $\mathbf{L}^\top \tilde{\mathbf{L}} = \mathbf{I}$ for $\tilde{\mathbf{L}}$ (i.e., $\tilde{\mathbf{L}} := \mathbf{L}^{-\top}$).
Update $\mathbf{A}_s^{-1} = \tilde{\mathbf{L}} \tilde{\mathbf{\Gamma}}$ and its transpose $\mathbf{A}_s^{-\top} = \tilde{\mathbf{\Gamma}}^\top \tilde{\mathbf{L}}^\top$ (required by the proposal distribution).

Algorithm 3 Adaptive Coordinate Rescaling (AdaCoRe) sampling scheme

Input: β and θ at the s -th iteration, the observed data $\mathbf{X} = (\mathbf{X}_1, \dots, \mathbf{X}_n)$, θ^* , $\xi = 0.05$, $\tau = 3/\sqrt{n}$ and $\varepsilon = 10^{-12}$. From the previous iteration $s - 1$: the cumulative sum $\Sigma_{l=1}^{s-1} \theta_l$, the current square root of Fisher information \mathbf{R}^* , and the exponential moving average $\bar{\delta}_{s-1}$. The notation $\|\cdot\|_F$ indicates the Frobenius norm of the matrix between bars.

if $s < S_{\text{burn-in}}$ **then** (INVERSE RESCALING MATRIX UPDATE)

 Update cumulative sum $\Sigma_{l=1}^s \theta_l = \Sigma_{l=1}^{s-1} \theta_l + \theta_s$

if $s > 1$ **then**

 Calculate relative curvature change $\delta_s = \frac{\|\mathbf{R}_s - \mathbf{R}^*\|_F}{\|\mathbf{R}^*\|_F + \varepsilon}$.

 Calculate exponential moving average $\bar{\delta}_s = (1 - \xi) \bar{\delta}_{s-1} + \xi \delta_s$.

if $\bar{\delta}_s > \tau$ **then**

 Update running mean $\bar{\theta}_s = \Sigma_{l=1}^s \theta_l / s$.

 Update \mathbf{A}^{-1} and $\mathbf{A}^{-\top}$ using **Algorithm 2**.

end if

end if

end if

Propose $\beta' \sim q(\cdot | \beta)$.

Calculate $\theta' = \mathbf{A}^{-1}(\beta' - \theta^*) + \theta^*$.

Calculate square root of inverse Fisher information \mathbf{R}' (see Appendix B).

Accept $\beta_{s+1} = \beta'$, $\theta_{s+1} = \theta'$ and $\mathbf{R}^* = \mathbf{R}'$ with probability

$$\alpha(\beta, \beta') = \min \left\{ 1, \frac{\tilde{f}(\mathbf{X}; \theta') \pi(\theta') q(\beta | \beta')}{\tilde{f}(\mathbf{X}; \theta) \pi(\theta) q(\beta' | \beta)} \right\},$$

otherwise reject and set $\beta_{s+1} = \beta$ and $\theta_{s+1} = \theta$.

next section, we present an adaptive CoRe sampling scheme, the AdaCoRe, where the inverse matrix \mathbf{A}^{-1} is estimated iteratively during the burn-in stage.

3.3 An adaptive version of the CoRe sampler

The adaptive version, AdaCoRe, does not require the researcher to provide a prior estimate of the rescaling matrix \mathbf{A} , but the matrices $\mathbf{\Gamma}$ and \mathbf{L}^\top are updated in real time, based on the running sample mean $\bar{\theta}$. The iterative estimation of \mathbf{A} aims to efficiently update the components that determine

$\mathbf{\Gamma}$ and \mathbf{L}^\top , which are: (i) the model Hessian matrix, \mathbf{H} , (ii) the variance of the score, \mathbf{U} , and (iii) the prior curvature, \mathbf{H}_θ . We propose an update routine of these components that is performed only during the chain’s warm up phase, ensuring detailed balance and convergence to the target posterior. Once the three components above are evaluated at the running mean $\bar{\theta}$, we then calculate $\mathbf{A}^{-1} = \mathbf{L}^{-\top} \mathbf{\Gamma}^{-1}$, where the inverse matrices $\mathbf{\Gamma}^{-1}$ and $\mathbf{L}^{-\top}$ are determined by solving linear systems, which is computationally more stable and faster than inverting the whole matrices. Furthermore, the update of the rescaling matrix is performed only when the relative change of the local curvature between two subsequent sampling iterations exceeds a threshold, which is set to $3/\sqrt{n}$.² For clarity, we provide the steps for updating the inverse matrix \mathbf{A}^{-1} in Algorithm 2, and the steps of the AdaCoRe sampler in Algorithm 3.

The attractive feature of the CoRe sampling methods lies in the combination of the pseudo-likelihood’s computational scalability with a principled correction for the posterior covariance structure via the rescaling matrix. As will be illustrated later, this results in a sampler that is capable of exploring regions of the parameter space that would have low probability under the pseudo posterior. To evaluate the efficiency and performance of the CoRe sampling methods, in the next section, we benchmark this new sampling scheme against established methods using simulated data.

4 Performance comparison with competing approaches

In the previous section, we introduced and discussed two sampling strategies that aim at improving the quality of posterior inference in discrete MRFs: the CoRe sampler with fixed rescaling matrix and its adaptive version, the AdaCoRe sampler, which updates the rescaling matrix in real time during the warm-up phase. Now, we need to evaluate their performance. With such a purpose, in this section, we compare the efficiency and performance of the two CoRe samplers with that of existing approaches. These approaches include sampling strategies from existing literature that are either readily available for Markov Random fields or adaptable to them. We divided the methods under comparison into three classes: (i) recalibration methods, which transform the pseudo posterior distributions to an adjusted covariance structure, (ii) approximations of the full likelihood, which define a surrogate function of the full likelihood, where the partition function is equal to the set of unique observed states, and (iii) approximations of the transition kernel, which estimate exact gradient and ratio of partition functions using Monte Carlo simulations. The three classes of methods described here are based on a common MCMC sampler, whose details are given in Appendix B. In the following subsections, we first describe the details of each class, then we introduce the simulation framework used to conduct the numerical experiments and present the corresponding results.

²The factor $1/\sqrt{n}$ reflects the typical magnitude of sampling variability of a Hessian function estimated from n independent observations. The threshold $3/\sqrt{n}$ is a conservative choice that prevents updates of the rescaling matrix due to random fluctuations.

Recalibration methods

We consider two methods that transform the pseudo posterior distribution to an adjusted covariance structure: the post hoc calibration methods, that rescale the draws sampled from the pseudo posterior, and alternative definitions of the Core sampling method, which are based on the same CoRe sampler in Algorithm 1 but differ on the definition of the rescaling matrix:

- **Post hoc calibration methods.** [Bouranis et al. \(2017\)](#) proposed a post hoc calibration for exponential random graph models. This method transforms the pseudo posterior draws by rescaling them to a new structure of variance and covariance. Thus, to rescale each draw $\boldsymbol{\theta}$ into a new vector of draws $\boldsymbol{\theta}_{\text{new}}$, we perform a transformation that first standardizes the draws, assigns a different scale to the parameters, and then shifts them back to their original location. The formula for such transformation is

$$\boldsymbol{\theta}_{\text{new}} = \mathbf{\Gamma} \mathbf{L}^\top (\boldsymbol{\theta} - \boldsymbol{\theta}^*) + \boldsymbol{\theta}^*,$$

where $\boldsymbol{\theta}^*$ is a location parameter, usually an unbiased posterior estimate of the model parameters (e.g., MAP estimates), \mathbf{L}^\top is the upper triangular from the Cholesky decomposition of the negative Hessian evaluated at $\boldsymbol{\theta}^*$, and $\mathbf{\Gamma}$ is the lower triangular from the Cholesky decomposition of the new variance and covariance structure for the parameters also evaluated at $\boldsymbol{\theta}^*$. The rescaling operates similar to the standardization of a random multivariate Normal distribution and aims to calibrate the posterior draws towards a resulting posterior distribution that is wider than the one based on the pseudo-likelihood function, where the new posterior variability corresponds to that of $\mathbf{\Gamma} \mathbf{\Gamma}^\top$.

In the original work of [Bouranis et al. \(2017\)](#) the post hoc calibration method determined the optimal parameters ($\boldsymbol{\theta}^*$) using the Robbins-Monro stochastic approximation method ([Robbins and Monro, 1951](#)), estimated the new posterior location and the covariance structure ($\mathbf{\Gamma} \mathbf{\Gamma}^\top$) from the full likelihood via Monte Carlo simulation. In our comparison, we consider this approach and we refer to it as Post Hoc calibration with Robbins-Monro (“PH-RM”). In addition to this, we also include two post hoc approaches that stem from the same idea but differ in how the new covariance structure or the optimal location parameters are determined. We introduce: (i) the Godambe-Huber-White approach (“PH-GHW”), which uses the same covariance matrix estimator discussed in Section 3.2, noted as $\boldsymbol{\Sigma}_{\text{GHW}}$, and (ii) the Monte Carlo Hessian method (“PH-MCH”), which estimates the covariance structure of the full likelihood via Monte Carlo simulation (akin to PH-RM). Finally, both post hoc variations center the posterior draws at the posterior means. To maintain readability, we omit the technical details of the post hoc methods and instead refer the reader to Appendix C, where

we discuss the estimation of the new covariance structure and outline key features, advantages and limitations of each post hoc method.

- **Alternative definitions of CoRe sampling.** Without loss of generality, we introduce two variants of the CoRe sampling scheme that use a fixed rescaling matrix. These variants differ on the type of rescaling matrix they use. The first variant, referred to as “CoRe-RM”, employs a covariance structure estimated through the Robbins-Monro algorithm ([Robbins and Monro, 1951](#)), where the model parameters are also optimized. The second variant, called “CoRe-MCH”, uses a covariance structure based on the full likelihood and estimated via Monte Carlo simulation at the posterior modes. Both variance structures are the same of those defined above for the two post hoc calibration methods PH-RM and PH-MCH.

Approximations of the full likelihood

We introduce here the empirical likelihood function, which is an approximation of the full likelihood. The definition of the empirical likelihood follows the result of [Hessen \(2023\)](#), which simplifies the modeling of categorical data when the support of the full population model is unknown. The simplification consists of deriving a subpopulation model whose support only accounts for the unique observed states. The restricted support makes the maximum likelihood estimation computationally efficient because the log-likelihood sums over at most the sample size. This method, referred to as “Empirical”, preserves more of the global structure than the pseudo-likelihood, while remaining computationally tractable. We write the empirical likelihood as,

$$f_{\text{empirical}}(\mathbf{X}; \boldsymbol{\theta}) = \frac{1}{Z_{\text{empirical}}(\boldsymbol{\theta})^n} \exp \{ \mathbf{s}(\mathbf{X})^\top \boldsymbol{\theta} \} \quad (4)$$

which is akin to the full likelihood of a discrete MRF as seen in Equation 1 and the only difference lies in the denominator, where the partition function $Z_{\text{empirical}}(\boldsymbol{\theta}) = \sum_{\mathbf{x}' \in \mathcal{X}_{\text{empirical}}} \exp \{ \mathbf{s}(\mathbf{x}')^\top \boldsymbol{\theta} \}$ is based on a different set of states, $\mathcal{X}_{\text{empirical}} \subseteq \mathcal{X}$, consisting only of the unique states observed in the data at hand. Although the definition of a simplified partition function noticeably reduces the computational burden of the denominator, our experiments indicate that, for discrete MRFs, the empirical likelihood introduces bias in the locations of the posterior distributions. However, we can address this issue by shifting the locations of the posterior distributions to the pseudo posterior modes.

Approximations of the transition kernel

We consider two methods that approximate the transition kernel via a double Metropolis-Hastings sampling scheme ([Murray et al., 2006; Park and Haran, 2018](#)). These approaches address the

computational challenges of doubly-intractable models by using approximate expectations on the full likelihood and adapting their proposal distribution iteratively. This adaptation is based on either an empirical estimate of the posterior covariance or by an iterative approximation of the Fisher information.

The first method is the Adaptive Double Metropolis-Hastings (“AdaDMH”), which iteratively updates the covariance matrix of the proposal distribution based on previous samples (Haario et al., 2001). Furthermore, a Gibbs sampler (inner Metropolis-Hastings) is used at each iteration to approximate the ratio between partition functions in the acceptance ratio step. The adaptive covariance structure is expected to improve the exploration of the target posterior while preserving the double Metropolis-Hastings structure. The sampling scheme of the AdaDMH is different from that used by the other methods and the details on its algorithm are provided in the Appendix D. The second method is a Double Metropolis-Hastings (in short, “DMH”), whose adaptive sampling scheme is illustrated in Appendix B. In this case, the within Gibbs sampling approximates both the ratio of partition functions and the full likelihood gradient, which is required by the proposal distribution.

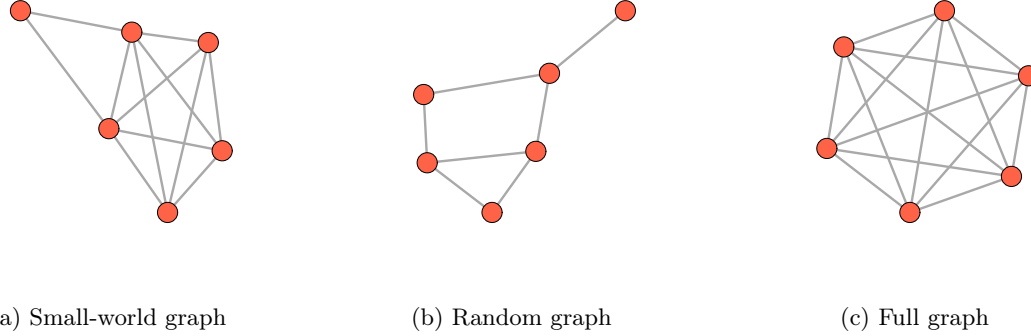


Figure 4: Examples of three graph structures for six nodes.

4.1 Numerical experiments: data, framework and metrics

In this section, we present a series of numerical experiments to evaluate the proposed methodology and to compare its performance with the methods introduced in the previous section. However, the specification of the model parameters in Markov Random fields is a nontrivial operation, as they control for complex dependency structures and have a non linear relation with the normalizing constant. Instead, we adopt a data-driven approach in which the parameters are first estimated from the observed data and then treated as the true parameters to generate random data. We considered data collected from a study on sexual compulsion and hypersexuality³. This study used the Sexual Compulsivity Scale (SCS) Kalichman and Rompa (1995), which was developed to evaluate

³data are available at http://openpsychometrics.org/_rawdata/ and last updated on 16 July 2012

tendencies related to hypersexuality. The data contains 3,376 observations and 13 variables, of which 10 variables (“Q1” to “Q10”) include questions related to descriptions of sexual behavior and are measured on a Likert scale (1=“Not at all like me”, 2=“Slightly like me”, 3=“Mainly like me”, 4=“Very much like me”). The remaining variables include the score (calculated as the sum of the answers to the 10 variables), the gender, and the age of the participants.

In our numerical experiments, we explore how posterior correction methods improve Bayesian inference in detecting the absence of interaction (conditional independence) between pairs of nodes. Thus, we examine three different types of network structure: (1) a small-world graph (Watts and Strogatz, 1998), (2) a random graph (Renyi, 1959) with a density of 0.3, and (3) a fully connected graph, which contains all possible edges between nodes (examples of random graph structures with 6 nodes can be found in Figure 4). We define two network sizes, 6 and 9, based on the number of nodes (P), where the number of parameters for a network with 9 nodes is almost twice the parameters in a network of 6 nodes. We also consider six sample sizes (N): 500, 1000, 1500, 2000, 2500, and 3000, each size increasing by 500 statistical units. Finally, we design a grid of 36 conditions based on the combination of the three structures, the two network sizes and the six sample sizes. Under each condition, we simulate 100 datasets following the steps outlined in Appendix E, where we explain how the original data were used to retrieve model parameters for data generation. For each method under comparison, we consider 25,000 iterations in a single chain, with 5,000 allocated to the burn-in phase. Finally, for each generated dataset, we estimate the full set of model parameters (thresholds and interactions), including the pairwise associations related to edges that are absent in the true data-generating networks with a “smallworld” or a “random” structure.

In the sampler presented in Appendix B, we initialize the (unnormalized) global variance parameter σ^2 parameter at 0.001 for the exact posterior sampling and at 1.0 for the pseudo posterior sampling, which is the standard value proposed by Titsias (2024). However, since this parameter is allowed to increase or decrease, we want to confirm that a different initialization for the exact posterior sampler did not deteriorate its performance. To this end, in Appendix ??, we report the trend of σ^2 for the pseudo posterior and the exact posterior sampler, for a random set of 5 networks from each of the 36 conditions. The initialization of σ^2 at 0.001 stabilizes over the iterations around the same range of values of the pseudo posterior sampler, not showing particular deviations. Furthermore, we set the number of Monte Carlo samples to 25,000 for the DMH and the AdaDMH, as their sampling routine requires within sample approximations at each iteration and a larger number of samples would affect the efficiency of both methods. Instead, we consider 100,000 Monte Carlo samples for the methods that require approximations of quantities out of the sampling stage, which include PH-RM, PH-MCH, CoRe-MH and CoRe-MCH.

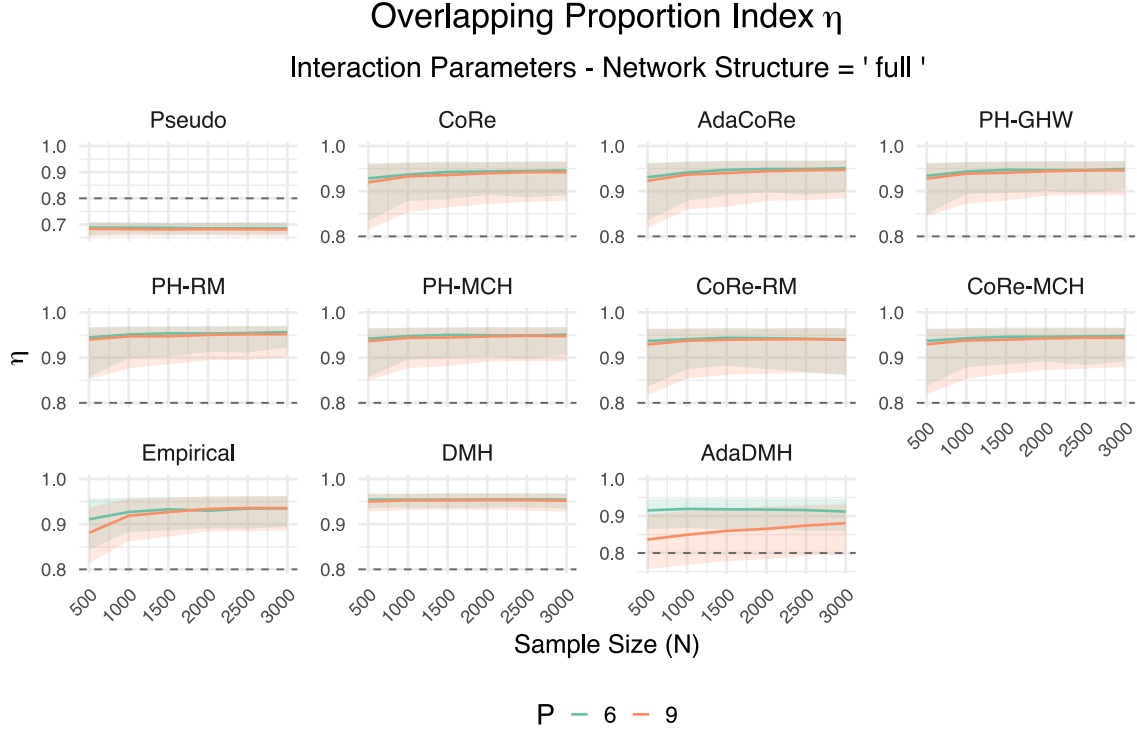


Figure 5: Overlapping proportion index η between exact and corrected posterior distributions for the interaction parameters in a network with “full” structure. The horizontal dashed gray line marks a reference level at 0.8.

We run the experiments on the Dutch national supercomputer Snellius⁴, where we dedicated an exclusive node with 192Gb memory to each study condition, and run the analysis of 100 simulated networks parallelized on 100 threads (one for each simulated network). The R (R Core Team, 2025) code for all the experiments is available at – LINK REMOVED FOR BLINDED REVIEW – . The methodology presented in this work is available via the R package – LINK REMOVED FOR BLINDED REVIEW – .

We evaluated several metrics to compare the performance of the correction methods against the exact posterior distribution. These metrics included the percentage of overlap between corrected and exact posterior density (Pastore and Calcagni, 2019), with higher values indicating greater similarity between the two distributions. We also considered the Bayes factor test for conditional independence using the Savage-Dickey density ratio (Heck, 2018; Mulder et al., 2020). The value of this ratio depends on the height of the posterior density at the null hypothesis’ value and provides a local measure of agreement between corrected and exact posterior density. Additionally, we analyzed the ratio of posterior standard deviations which offers a relative comparison of the uncertainty of posterior densities. Finally, we examined the effective sample size (ESS) and runtime (in seconds)

⁴<https://www.surf.nl/en/dutch-national-supercomputer-snellius>

for each method, measuring, respectively, the amount of independent information contained in the posterior samples and the computational cost required to generate them. We introduce each of these metrics in the following paragraphs.

Quantifying the overlapping between posterior distributions. To measure the amount of overlapping area between two distributions, we consider the distribution-free index introduced by [Pastore and Calcagnì \(2019\)](#). This index quantifies differences between samples without relying on stringent distributional assumptions. We focus on the normalized version of the overlapping index η which is calculated for the single model parameter θ as

$$\eta(\pi^*(\theta|\mathbf{X}), \tilde{\pi}(\theta|\mathbf{X})) = \int_{\mathbb{R}} \min [\pi^*(\theta|\mathbf{X}), \tilde{\pi}(\theta|\mathbf{X})] d\theta$$

where $\pi^*(\theta|\mathbf{X})$ is our target posterior distribution (exact posterior), and $\tilde{\pi}(\theta|\mathbf{X})$ is an approximation of the target posterior π^* resulting from one of the methods under comparison. The normalized version of the η index assumes values in $[0, 1]$, with 0 indicating no overlap between the two distributions and 1 indicating perfect overlap. Furthermore, since we rely on posterior draws from both the exact posterior distribution and the posterior derived from the correction methods, we work with a discretized version of both densities. As a result, we can adapt the integral to this discretization and convert it into a summation over the unified support of both densities. For further details on discretization of the η index, we refer the reader to the work of [Pastore and Calcagnì \(2019\)](#).

Testing for absent edges via Savage-Dickey density ratio. The Savage-Dickey density ratio is a method of Bayesian inference used to compute Bayes factors for the comparison of nested models ([Heck, 2018](#); [Mulder et al., 2020](#)). In this specific case, the Bayes Factor is usually expressed as the posterior to prior ratio evaluated at a specific parameter value (usually a value under the hypothesis that one wants to test for.) We can take advantage of the posterior samples and calculate the Bayes factor to test the constrained hypothesis $\mathcal{H}_c : \theta = 0$ against an unconstrained one $\mathcal{H}_u : \theta \in \mathbb{R}$, with the simplified formula

$$BF_{cu} = \frac{\pi(\theta = 0|\mathbf{X})}{\pi(\theta = 0)}$$

where $\pi(\theta = 0|\mathbf{X})$ is the posterior density of θ evaluated at 0, and $\pi(\theta = 0)$ is the prior density of the same parameter evaluated at 0. In our numerical experiments, the numerator is calculated for all the posterior distributions resulting from methods under comparison and for the exact posterior. The denominator is calculated using the prior distributions assumed for the model parameters, which are discussed in [Appendix B](#).

Moreover, here we consider the use of the Savage-Dickey density ratio as one of the possible methods to test conditional independence between nodes in a Bayesian network. Other Bayesian testing approaches for assessing conditional independence within psychometric networks are examined by

[Sekulovski et al. \(2024\)](#). It is important to clarify that the Savage-Dickey ratio can be seen as a preliminary method to test conditional independence in a simplified framework where we do not need to compute or approximate integrals. However, the choice of the prior can strongly affect the accuracy of the Bayes factor. Indeed, with the Savage-Dickey ratio we can calculate an accurate Bayes factor only when the prior distribution of the nuisance parameters (ψ) in the nested model (\mathcal{H}_c) matches the conditional prior distribution in the full model (\mathcal{H}_u), that is $\pi(\psi | \mathcal{H}_c) = \pi(\psi | \theta = 0, \mathcal{H}_u)$.

We tested $\theta = 0$ for those interaction parameters that in the true data-generating network were indeed 0. In other terms, we tested the conditional independence for the truly absent edges in the networks with “random” and “smallworld” structures. With this choice we directly assess the extent to which each method correctly favors the hypothesis of conditional independence when it is true. Since no considerable differences in the results were observed between the two network structures, the discussion of this metric will focus on the “random” network structure. Illustrations for the “smallworld” structure can be found in the Supplementary Material.

Ratio of posterior standard deviations. We considered only the network structures “smallworld” and “random”, which admit conditional independence relations, and focused the analysis on the posterior distribution of parameters associated with edges that are absent in the corresponding true data-generating network. We chose these specific parameters for two reasons: the comparison between scales is not influenced by variations in the true effect size and the scale of these distributions directly influences the height of the Savage-Dickey density ratio, which supports the findings from the comparison of the density ratios. First, we calculated the standard deviation under each correction method (σ_{method}). Then, we considered the exact posterior distribution of the same parameter, measured its standard deviation (σ_{exact}) and calculated the ratio $\sigma_{\text{method}}/\sigma_{\text{exact}}$, for each correction method. A ratio higher (lower) than 1.0 indicates greater (smaller) uncertainty for the approximated posterior of a specific method compared to that of the exact posterior.

Effective sample size and runtime. We calculated the effective sample size (ESS) for each parameter using the R package ‘coda’ ([Plummer et al., 2006](#)) and recorded the wall-clock time spent sampling 25,000 draws.

In the next section, we present the results for each metric with a focus on the interaction parameters. Finally, we conclude with a summary discussion that condenses the findings from the three metrics. Additional summary figures on the results for the threshold parameters are provided in the Supplementary Material. Whenever we introduce line plots with shaded regions: the line represents the median value of the measure calculated on the 100 simulated networks, while the shaded region represents the 90% data range (i.e., the 5th to 95th percentiles).

4.2 Performance evaluation and simulation results

We present the simulation results and the performance analysis for each metric, following the order in which we introduced them. In Figure 5, we present the distribution of the index η for the interaction parameters across P and N in the case of a full network structure. We observe that, across all calibration methods, the overlap between the true target and the corrected posterior distribution improves when compared to the pseudo posterior distribution. Specifically, the pseudo posterior density overlaps with the exact posterior by approximately 65% to 70%, while the median overlap of the calibration methods exceeds 80%. Both the post hoc calibration and coordinate-rescaling methods achieve a median overlap of between 90% and 95%. The Empirical method reaches a median overlap slightly below 95% but only when the sample size is increased. This trend indicates that the performance of the method is dependent on the number of unique states observed in the sample, which is used to approximate the intractable partition function. Additionally, there is a notable discrepancy in performance between DMH and AdaDMH, the two methods approximating the transition kernel. The DMH is the best performing method under overlapping index metric, as the proportion remains stable with little variability around 95% across network and sample sizes. On the other hand, the performance of the AdaDMH drops from consistently above 90% with 6 variables (green line) to a value lower than 85% when the number of variables increases to 9 (orange line). In the latter case, the index shows a gradual increase towards 90% but with a greater variability than the scenario with 6 variables. Both adaptive samplers are compared under identical settings, using 25,000 iterations in the inner Gibbs sampling step. The only difference between them lies in the proposal distribution: the proposal of the DMH adapts to the local curvature through Fisher information and builds around an adaptive Langevin process, the AdaDMH defines an adaptive multivariate normal random walk as proposal, which learns the curvature using the running samples, starting from a robust estimate of the covariance structure (via a sandwich estimator) and gradually blending it to the learned one. As the complexity of the model increases from 6 to 9 nodes, for all methods we observe a noticeable increase in the variability of the overlap index, especially at smaller sample sizes. This higher variability is expected, as the model parameters have almost doubled, increasing the complexity of the model. For a more detailed assessment, the performance of the overlapping index is presented in the Supplementary Material, both for the remaining network structures (“random” and “smallworld”) and for the threshold parameters of a full network structure. The results remain consistent, with the only difference that the exact posterior of the threshold parameters is well approximated by the pseudo posterior (the median overlapping index is above 80%) but the calibration methods still outperform it, reaching a median above 90%. Finally, the variability across simulations reduces when considering networks with missing edges (“random” and “smallworld”).

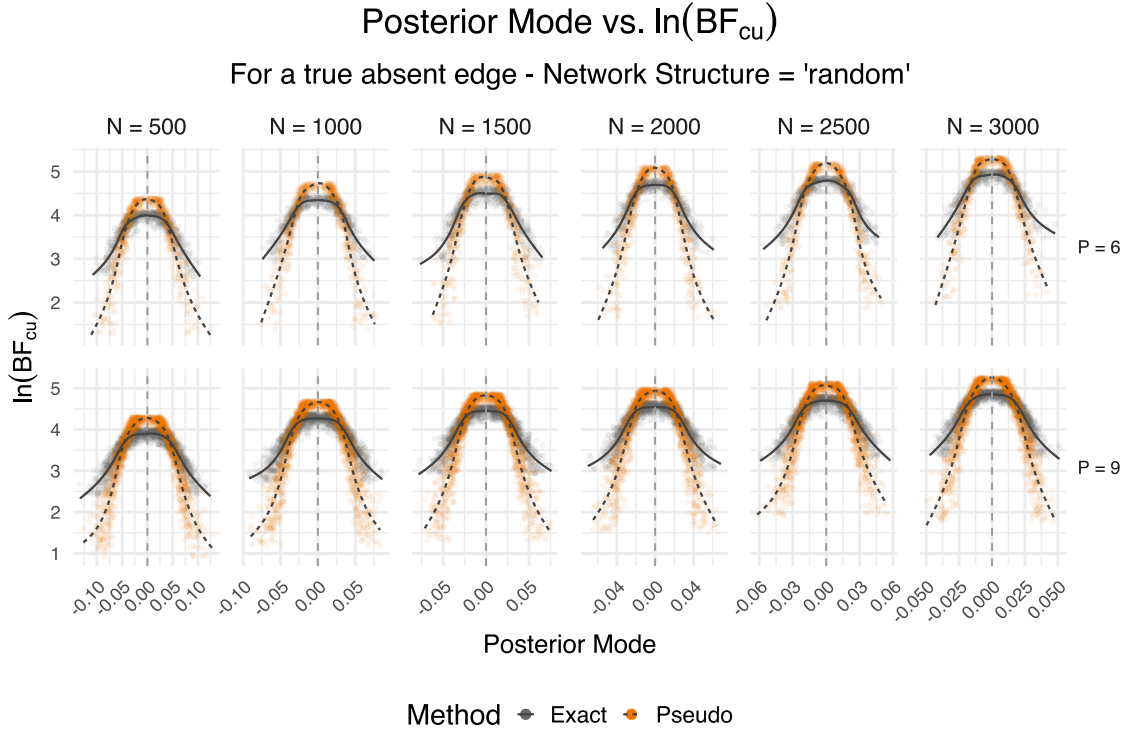


Figure 6: Scatterplot of posterior mode versus $\ln(BF_{cu})$ (Savage-Dickey log-density ratio) for a true absent edge in a “random” network structure, based on results from the exact and pseudo posterior methods. Rows correspond to different network sizes (P) and columns to different sample sizes (N). Trends are indicated with black lines: a solid line for the exact posterior and a dashed line for the pseudo posterior.

To analyze the results of the simulation studies on the Savage-Dickey density ratio, we first consider the natural logarithm of the ratio and compare the log-density ratio calculated using the exact posterior to that calculated with the pseudo posterior. This comparison already highlights the efficiency loss of the pseudo posterior when testing for conditional independence for edges that are absent in the true data-generating network. Next, we examine the performance of the calibration methods in comparison to the log-density ratio from the exact posterior. In Figure 6, we present the scatter plot that describes the relationship between the posterior mode of the interaction parameter estimated for a true absent edge and the natural logarithm of the corresponding Savage-Dickey density ratio. We observe this relationship across sample sizes (N) and network sizes (P) for both pseudo posterior (in orange) and exact posterior (in gray). The black lines indicate the trend of the two scatter plots and illustrate a consistent behavior of the pseudo posterior across different network structures, P and N . When the estimate of the posterior mode is distant from zero, the log-density ratio for the pseudo posterior results in a lower value than that of the exact posterior. Conversely, as the estimated posterior mode approaches zero, the log-density ratio for the pseudo posterior becomes significantly higher than the exact posterior. Both relationships arise from the

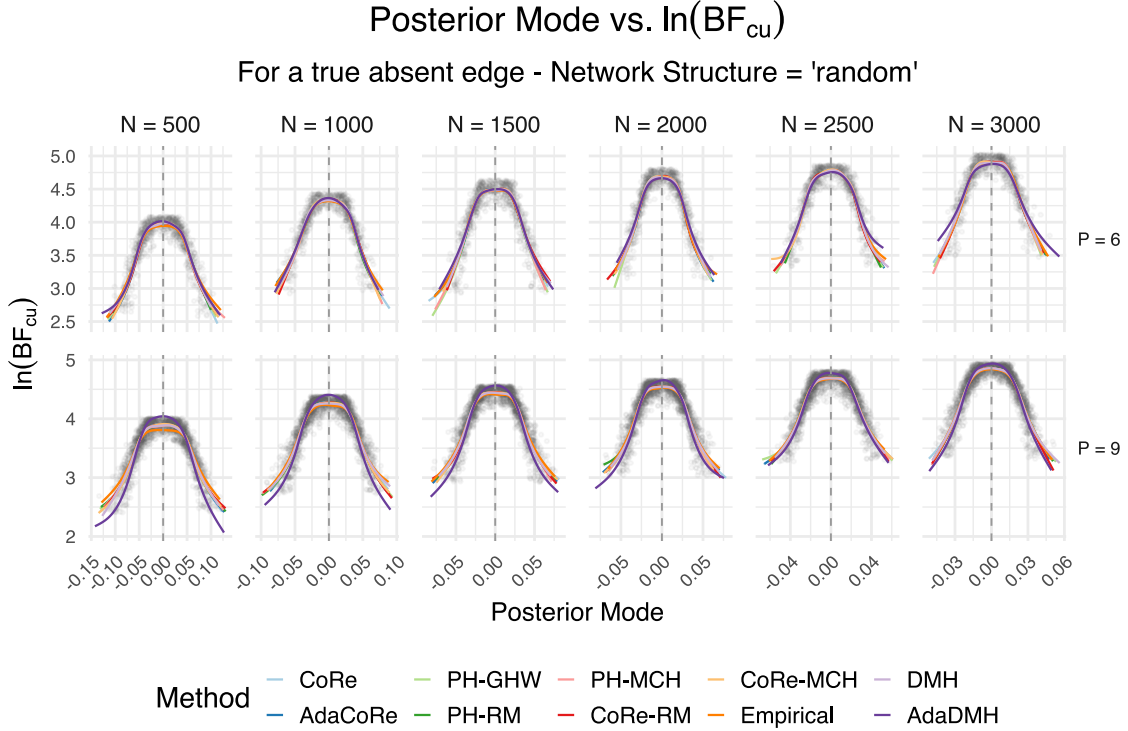


Figure 7: Trend lines of posterior mode versus $\ln(BF_{cu})$ (Savage-Dickey log-density ratio) across calibration methods for a true absent edge in a “random” network structure. Rows correspond to different network sizes (P) and columns to different sample sizes (N). The dark gray dots show the scatterplot of the same quantities for the exact method.

underestimated variability in the pseudo posterior, which leads to lower log-density ratios when the posterior mode is distant from zero. At the same time, it inflates the ratio when the posterior mode is near zero. The areas of intersection between the two scatter plots represent the only regions where the magnitudes of the two ratios are similar and the methods align, which represents a small area. In Figure 7, we illustrate a similar scatter plot but for the remaining calibration methods. We only display the scatter plot for the exact method along with the trends of the calibration methods (excluding the pseudo posterior). On average, we observe that the magnitude of the log-density ratios aligns with that of the exact posterior across most methods. However, the AdaDMH and Empirical methods stand out, showing deviations from the remaining methods. The AdaDMH method follows a trend similar to that of the pseudo posterior, characterized by a peak when the posterior mode is near zero and lower values in the tails when the modes are farther from zero. In contrast, the Empirical method shows a lower trend near zero but higher tails for posterior modes that are away from zero. For each method, this behavior is more pronounced for smaller sample sizes and larger network sizes.

To support the findings from the comparison of log-density ratios, Figure 8 illustrates the trend of the ratio between pseudo posterior variability and exact posterior variability of the interaction

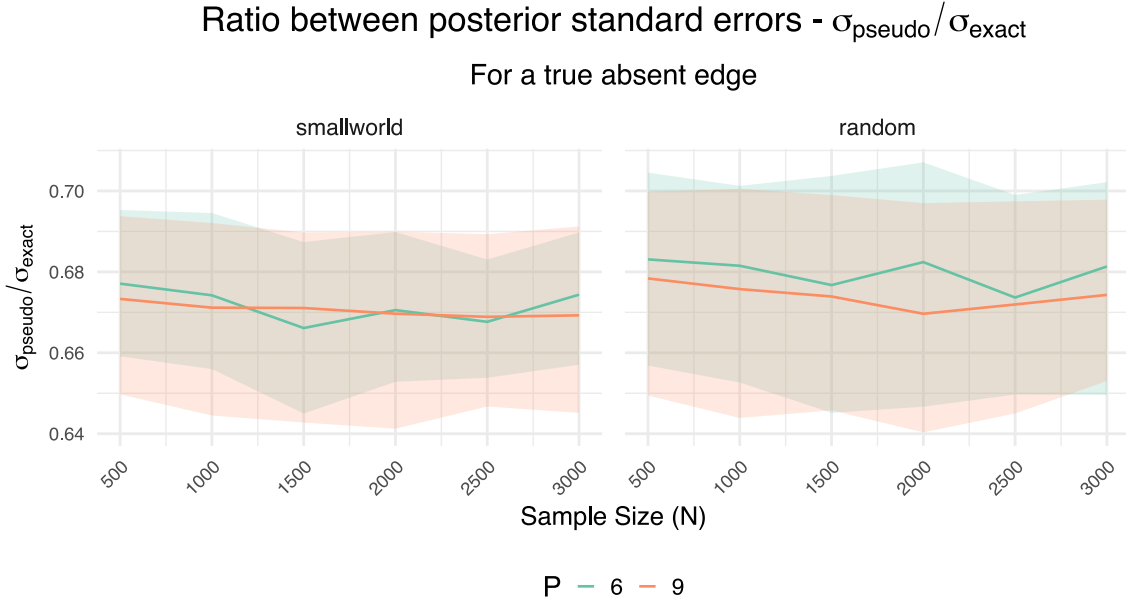


Figure 8: Ratio between the pseudo posterior standard error and the exact standard error ($\sigma_{\text{pseudo}}/\sigma_{\text{exact}}$) for a true absent edge in both “smallworld” and “random” network structure.

parameters shown in Figure 6 (true absent edges). It is evident that across the different sizes of N , P , and network structures, the pseudo posterior variability is consistently between 30% and 35% lower than the exact posterior variability. Figure 9 shows the same trend for all calibration methods, including the pseudo posterior. The core rescaling methods (CoRe and AdaCoRe), their alternative definitions (CoRe-RM and CoRe-MCC) and the PH-GHW are the best performing methods, whose median ratio is consistently close to 1.0, regardless sample size (N) and network size (P). For Core, AdaCoRe and PH-GHW, we observe that the variability around the median ratio decreases with the sample size and stabilizes around the same range of CoRe-RM and CoRe-MCH.

The performance of the remaining correction methods appears less optimal. We observe that in the PH-RM and PH-MCH methods, the median ratio is larger than 1.0 for small sample sizes, indicating an overestimation of the posterior variability, which diminishes as the sample size increases. The median ratio for the DMH is constantly above 1.0, which is not desirable, and its variability across replicates increases as the network size grows from six to nine nodes (orange shaded area). The AdaDMH and Empirical methods perform the worst, but for different reasons. The Empirical method initially overestimates the posterior variability, with a ratio greater than 1.0, and approaches 1.0 as the sample size increases. This result is directly related to the approximation of the partition function, which becomes more accurate with larger sample sizes. In contrast, in the AdaDMH, the ratio fails to stabilize around 1.0 in both network sizes. The situation worsens when $P = 9$, with the ratio barely reaching 1.0. This poor performance is likely due to the non-optimal exploration performed by

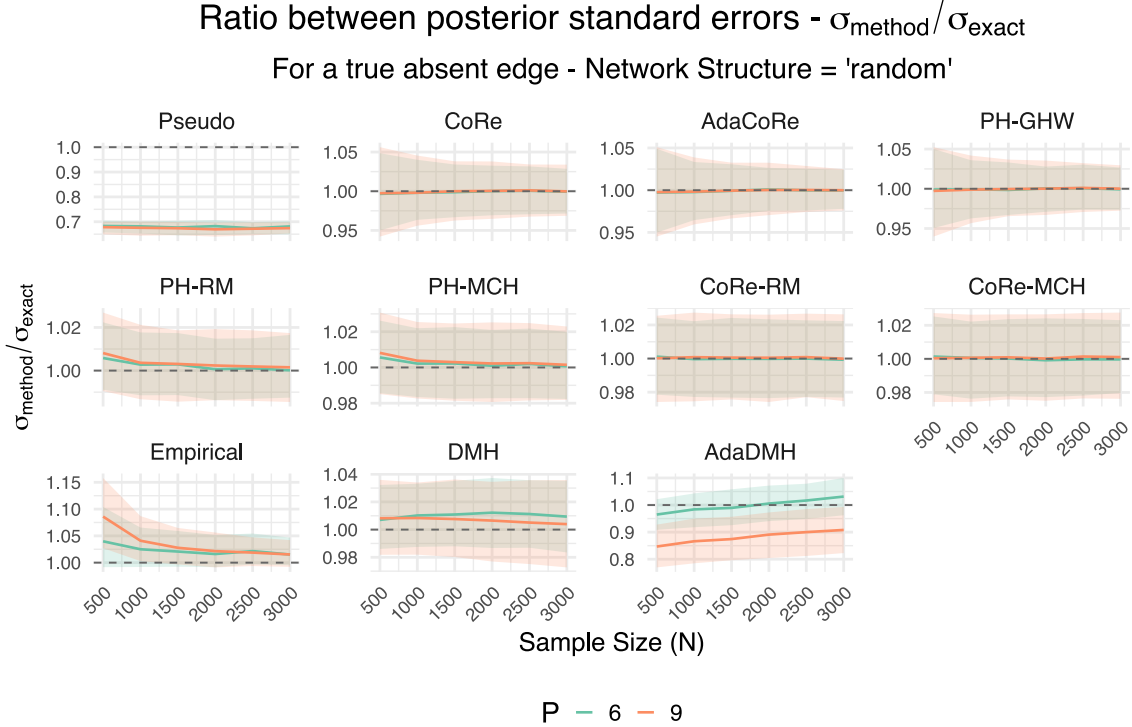


Figure 9: Ratio between the corrected posterior standard error and the exact standard error ($\sigma_{\text{method}} / \sigma_{\text{exact}}$) for a true absent edge in a network with “random” structure, illustrated for all calibration methods. The horizontal dashed gray line marks a reference level at 1.0, where the posterior standard errors are the same.

the proposal. Unlike the AdaDMH, all correction methods, including the pseudo posterior and the exact method, are built around an adaptive proposal that learns the local curvature of the posterior, improving the exploration of the posterior space. The trend of the ratio for the Empirical and the AdaDMH methods confirm the results shown in Figure 6, indicating a mismatch in the log-density ratios of the two calibration methods compared to the exact method.

Table 1: Effective Sample Size (ESS) for network structure = “full”

Method	N	P = 6				P = 9			
		500	1,500	2,500	3,000	500	1,500	2,500	3,000
Exact		3,109	3,250	3,276	3,281	2,276	2,429	2,459	2,470
Pseudo		3,289	3,308	3,319	3,321	2,478	2,500	2,504	2,509
PH-RM		3,290	3,309	3,320	3,320	2,479	2,501	2,506	2,509
PH-GHW		3,292	3,315	3,320	3,322	2,482	2,503	2,506	2,509
PH-MCH		3,293	3,315	3,319	3,321	2,484	2,504	2,507	2,510
CoRe		3,295	3,324	3,327	3,330	2,490	2,507	2,511	2,517
CoRe-RM		3,290	3,323	3,327	3,330	2,483	2,510	2,514	2,518
CoRe-MCH		3,291	3,311	3,325	3,329	2,485	2,509	2,510	2,516
AdaCoRe		3,300	3,319	3,324	3,329	2,485	2,510	2,511	2,513
Empirical		3,094	3,253	3,277	3,279	2,230	2,415	2,450	2,461
DMH		3,148	2,651	2,117	1,902	2,474	1,870	1,283	1,094
AdaDMH		220	217	214	213	148	146	145	143

Note: highlighted cells indicate the highest value in each column.

Table 2: Runtime (seconds) for network structure = “full”

Method	N	P = 6				P = 9			
		500	1,500	2,500	3,000	500	1,500	2,500	3,000
Exact		2.55	2.58	2.53	2.48	906.33	906.19	913.14	901.53
Pseudo		17.21	50.73	84.62	101.70	31.70	93.47	156.83	187.43
PH-RM		17.92	51.59	87.55	105.27	32.67	94.65	157.05	190.42
PH-GHW		17.48	51.08	84.92	101.63	31.86	93.96	155.78	187.93
PH-MCH		17.72	51.15	84.91	101.66	32.51	94.49	156.35	188.25
CoRe		34.03	101.43	169.05	205.65	62.71	189.12	310.75	372.25
CoRe-RM		34.08	101.24	170.45	207.42	63.32	187.13	310.40	372.15
CoRe-MCH		34.04	101.19	169.10	205.62	62.80	186.67	310.06	374.92
AdaCoRe		38.55	114.81	190.72	228.51	77.6	236.12	396.34	474.86
Empirical		0.42	0.61	0.73	0.76	0.90	1.49	2.87	3.20
DMH		2,358.95	2,356.25	2,366.87	2,378.93	3,820.18	3,815.51	3,827.16	3,823.08
AdaDMH		2,340.74	2,343.53	2,354.05	2,361.56	3,808.72	3,801.85	3,814.29	3,808.18

The computational efficiency of the methods is assessed in terms of effective sample size and their runtime. We observed that there were no significant differences in ESS and runtime among the three network structures tested. Therefore, we will focus our discussion on the results specifically for networks simulated using the “full” network structure, which are detailed in Tables 1 and 2. Tables for the “smallworld” and “random” network structures are provided in the Supplementary Material.

Table 1 illustrates the median ESS for a subset of sample sizes ($N = \{500, 1500, 2500, 3000\}$), network sizes ($P = \{6, 9\}$), and for the “full” network structure, highlighting in bold the best (or equally best) performing method by column. The ESS describes the amount of independent information contained in the posterior draws, with higher values indicating better sampling efficiency. In general, higher ESS values are preferred, with the best ESS value being equal to the number of posterior samples. For all methods examined, we noted a drop in median ESS when increasing the network size from 6 to 9 variables. This observation aligns with our expectations, as model complexity increases with the number of parameters. While post hoc and coordinate-rescaling methods maintain a consistent ESS with increasing sample sizes (N), we observed a small increase in ESS for the Exact and the Empirical methods when transitioning from $N = 500$ to larger sample sizes. In contrast, the DMH and AdaDMH methods exhibited a decreasing trend in ESS. The performance of the DMH deteriorated as N increased, resulting in a drop of more than 1,200 effective samples when moving from $N = 500$ to $N = 3000$ across both network sizes. This decline may be attributed to increased noise from approximating the gradient and the ratio of partition functions at larger sample sizes. The AdaDMH produced the lowest effective sample size, indicating that the adaptive sampler yielded poor-quality samples with high autocorrelation. Overall, such a result indicates that the most effective methods are those whose samplers do not rely on approximating expectations via Monte Carlo simulation and whose covariance structure remains independent of the running states of the Markov chain.

In Table 2, we evaluated the computational burden associated with the calibration methods by measuring the median runtime in seconds, with shorter runtime indicating better computational efficiency. Since the performance is similar across different network structures, we will focus our discussion on the runtime results specifically for networks simulated using the “full” structure. Although we observe an increase in runtime when working with 9 variables, the extent of this behavior varies across methods. The most significant increase occurs with the Exact method, where the median runtime rises from approximately 2.5 seconds with $P = 6$, to over 900 seconds (more than 300 times slower) with $P = 9$. Additionally, we observe that, under each network size, the runtime of the exact sampler remains constant across sample sizes, meaning that the computational efficiency of the algorithm is mainly affected by the number of variables in the model, which determines the complexity of the partition function. The pseudo posterior sampler and the post hoc methods show comparable performance among them, since the post hoc calibration requires little amount of additional time to transform pseudo posterior samples. When the number of variables increases from 6 to 9 variables, the runtime approximately doubles, and, under each network size, the increase of runtime over sample sizes is nonlinear. The coordinate-rescaling methods take approximately twice as long as the post hoc rescaling methods, as indicated by the doubled runtime (across network and sample sizes). Similar to the post hoc methods, their runtime exhibits an increasing trend as the sample size (N) increases, suggesting that larger sample sizes lead to greater computational burden. The Empirical method is the fastest method, taking less than a second to run when $P = 6$, and with an increase in runtime of about 3 seconds when $P = 9$. The least efficient methods are the DMH and the AdaDMH, requiring between 38 minutes and slightly more than 1 hour to run a single chain. While the median runtime of the DMH remains consistent over N , its effective sample size decreases as N increases, reducing the sampling efficiency of the method. In contrast, the relation between the effective sample size of the AdaDMH and its runtime does not change significantly. The difference in computational efficiency between the two double Metropolis-Hastings algorithms is due to the different proposal distribution. In the DMH the efficiency decreases with N because the sampling scheme required the Monte Carlo approximation of both the exact gradient and the ratio of partition functions. In contrast, in the AdaDMH, only the acceptance ratio requires a Monte Carlo approximation.

4.3 Summary of findings

We conclude the analysis with a summary of the main insights gained from the simulation results across all metrics. The methods that perform the worst are the DMH, the AdaDMH and the Empirical method. Despite their overall poor performance in ESS and runtime, the DMH method shows the best trend in the overlapping index metric, consistently achieving around 95% with little variability

across the simulated datasets. While the magnitude of the DMH’s Savage-Dickey density-ratio aligns closely with that of the exact posterior, the magnitude of the Empirical and the AdaDMH methods deviates from it. The three methods altogether reveal a less desirable performance when considering the ratio between posterior standard errors. Both Empirical and DMH consistently overestimate the posterior variability, while the AdaDMH underestimates the variability for lower sample sizes and overestimates it for larger sample sizes. In terms of effective sample size and runtime, we can separate the three samplers into two distinct levels of efficiency. On one hand, the Empirical method stands out as the most efficient, with an effective sample size comparable to that of the post hoc and CoRe methods and the lowest median runtime observed among all the methods under comparison. On the other hand, the DMH and the AdaDMH are the least efficient ones, requiring a median runtime of between 38 and 65 minutes for a single-chain to run. The within-sampler Monte Carlo approximations used by the DMH and the AdaDMH result in longer waiting times, thereby reducing their computational efficiency.

Post hoc and CoRe methods show comparable performance in approximating the exact posterior distribution, as indicated by the results of the overlapping index, the Savage-Dickey test and the ratio between posterior standard errors. Although the Empirical method is notably faster, post hoc and CoRe methods achieve reasonable sampling efficiency, emerging as the most efficient and correct to address the limitations of pseudo posterior sampling.

5 Discussion

The main objective of this work was to develop sampling methods that maintain the computational scalability of the pseudo-likelihood of an ordinal MRF, while providing robust Bayesian inference about the network structure. We achieved this by introducing the CoRe methods, a sampling technique that generates draws from a rotation of the target distribution, approximating the uncertainty of the exact posterior. Next to the standard algorithm, which requires a fixed rescaling matrix, we also defined an adaptive version of the same, where the rescaling matrix is updated during the warm-up phase. The adaptive version is especially appealing because of its built-in adaptive rescaling routine, which removes the need for external approximations. In addition to this new approach, we provided a simulation study to compare the performance of the CoRe methodology against different classes of existing approaches that approximate the exact posterior. We measured the performance of each method on the basis of several distinct metrics that compared the calibrated posterior to the exact posterior density under different aspects. These metrics included: the overlapping proportion between calibrated and exact posterior distributions, the alignment in magnitude of the Savage-Dickey density ratio, the ratio between posterior standard errors, the effective sample size, and the runtime. The methods approximating the full likelihood (Empirical) and those approximating the transition kernel

(DMH and AdaDMH) performed the worst, but for different reasons. The former excelled in sampling efficiency (low runtime and large effective sample size) but showed less desirable performance in matching the exact posterior density and testing for conditional independence. The performance of the latter was undermined by the heavy computational burden, causing loss of efficiency (both DMH and AdaDMH), by the extremely low sampling efficiency and the deviation of the Savage-Dickey density ratio (AdaDMH). On contrary, The proposed CoRe methodology (CoRe and AdaCoRe), its alternative definitions (CoRe-RM and CoRe-MCH), and the post hoc calibration methods (PH-RM, PH-GHW and PH-MCH) demonstrated a consistently satisfactory performance under all the considered metrics. This suggests that such methods can be recommended for conducting reliable and efficient Bayesian inference in discrete MRFs. However, the applicability of the CoRe methodology and the post hoc methods depends on which strategy we choose to estimate the network structure. In this work, we conducted inference on the network structure after estimating the full set of parameters, including the interaction parameters associated with the pairwise associations that were absent in the generating network. We then focused our analysis on such interaction parameters, with the scope of comparing the efficiency of correction methods when the conditional independence is true under the generating model. In the following paragraph, we explain how the applicability of the post hoc and CoRe methods differ when we use a different strategy for the estimation of the network structure, and motivate why the CoRe methods offer a more flexible approach to this.

Post hoc calibration methods provide a practical solution by transforming existing pseudo posterior samples, making them particularly appealing in scenarios where re-running a sampler is computationally expensive. However, their application is limited to the context where the focus is the posterior distribution of the parameters and the estimation of the network structure is not an integrated part of the sampling algorithm but is carried out post estimation. CoRe methods benefit from two particular features that are missing in the post hoc approaches. First, they explore a broader posterior distribution during sampling, offering a robust posterior exploration. Second, they can be combined with edge selection algorithms, which jointly estimate parameters and network structure, operating on an optimal parameters' scale. Although the combination of edge selection algorithms with posterior correction methods goes beyond the scope of this work, we believe that these two features make coordinate-rescaling methods a more flexible and desirable technique for future work conducting edge selection while sampling.

Beyond the metrics and the network structure estimation discussed above, the specific MCMC sampler used for all the methods is a key factor that also influenced the overall performance and we discuss this next. All of the methods under comparison, with the exception of AdaDMH and including the exact method, used the same sampler. It stands out that learning the local geometry of the pseudo posterior or the approximated exact posterior improved the exploration of the posterior space,

resulting in larger effective sample size across methods. A proposal distribution that adapts after the local posterior curvature using a Fisher-information based approach is a promising initial strategy for future innovative techniques that, under minimal assumptions, can effectively approximate the exact posterior distribution.

The methodology and the results presented in this paper suggest several directions for future research. Our comparative analysis between methods indicates that the choice of the correction method involves a trade-off between computational efficiency, accuracy and robustness. This trade-off is well addressed by the coordinate-rescaling methods, which provide a strong foundation for future techniques. For instance, using alternative definitions of composite likelihood functions may retain more information of the full joint distribution and potentially outperform the pseudo-likelihood function. Another approach may be based on a definition of a surrogate likelihood that models the maximal cliques in a graph. Finally, the methodology behind the coordinate-rescaling approach can be generalized to other modeling frameworks where the full likelihood is typically approximated by a composite likelihood in the context of large systems, such as Gaussian Graphical Models (GGMs), Exponential Random Graph Models (ERGMs), Potts models, and Spatial Autoregressive Models (SAR), to name a few.

Acknowledgement

This work was supported by an ERC [GRANT NAME] (PROJECT-NUMBER-XXXX).

Competing interests

None.

Supplementary Material

Supplementary Material associated with this article can be found at: [OSF/repository].

A Posterior correlations: comparison between pseudo posterior correlations and CoRe correlations

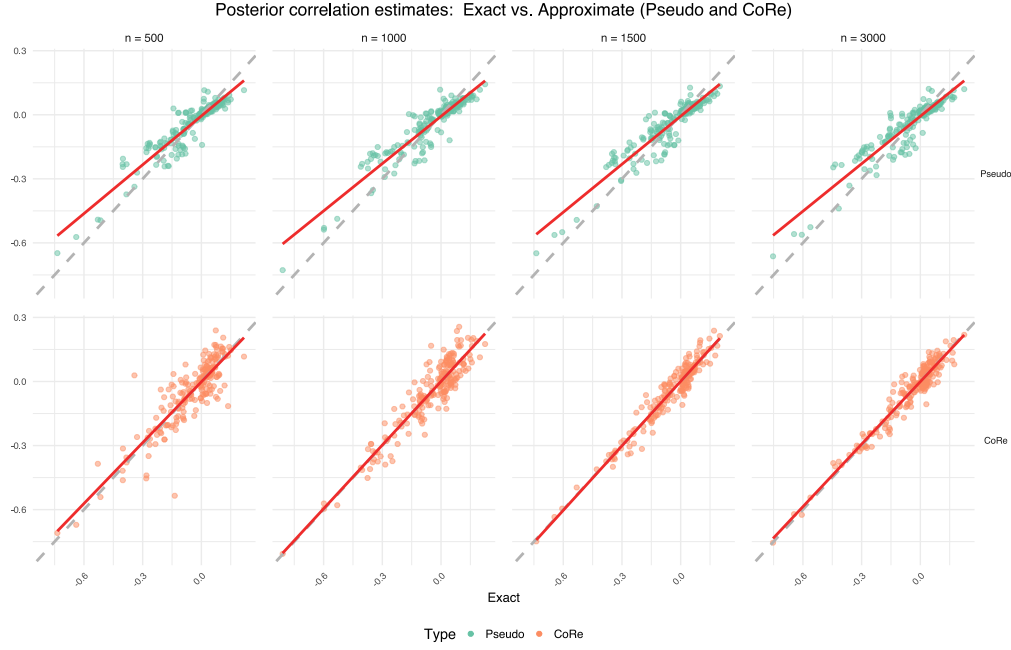


Figure A1: Comparison between approximate and exact posterior correlations over increasing sample size (n , by column) for a random network of $P = 6$ variables. (Top row) Pseudo posterior vs. exact posterior correlations result biased (not aligned to the dashed gray line). (Bottom row) CoRe posterior correlations vs. exact posterior correlations are unbiased but with a slight increase in variability that reduces with the sample size.

B The FisherMHALA sampling algorithm, and the prior distributions

Appendix to be added.

C Post hoc calibration: methodological details and implementation

Appendix to be added.

D The Adaptive Double Metropolis Hastings (AdaDMH) algorithm

Appendix to be added.

E Framework for dataset simulation and analysis

To generate the dataset $\mathbf{Y}_{i,j} \sim p(\cdot | \hat{\boldsymbol{\theta}}_i)$ using Gibbs sampling, we start the sampler at $\tilde{\mathbf{X}}_i$, that is the matrix consisting of N rows and P columns, randomly sampled from the data \mathbf{X} at iteration

Algorithm 4 Simulate 100 random datasets given sample size, network size and structure type

Input: the observed data $\mathbf{X} = (\mathbf{X}_1, \dots, \mathbf{X}_n)$, the sample size N , the network size P , the type of network structure \mathcal{S} , the number of random structures $K_{\text{str}} = 10$ to generate with type \mathcal{S} , the number of random datasets $K_{\text{sample}} = 10$ to simulate per each random structure, an empty list \mathcal{D} where to store simulated datasets.

Output: list of simulated datasets \mathcal{D} , each dataset is a matrix of dimensions $N \times P$.

```

for  $i \leftarrow 1$  to  $K_{\text{str}}$  do
  Generate random network structure  $s_i$  following structure type  $\mathcal{S}$ .
  Sample  $N$  observations  $\mathbf{r}_i$  with replacement from the row indices of  $\mathbf{X}$ .
  Sample  $P$  variables  $\mathbf{c}_i$  without replacement from the column indices of  $\mathbf{X}$ .
  Extract submatrix  $\tilde{\mathbf{X}}_i \leftarrow \mathbf{X}[\mathbf{r}_i, \mathbf{c}_i]$ .
  Estimate model parameters  $\hat{\boldsymbol{\theta}}_i \leftarrow \arg \max_{\boldsymbol{\theta}} \tilde{f}(\tilde{\mathbf{X}}_i; \boldsymbol{\theta})$  subject to  $\mathcal{S} = s_i$ .
  for  $j \leftarrow 1$  to  $K_{\text{sample}}$  do
    Generate dataset  $\mathbf{Y}_{i,j} \sim p(\cdot | \hat{\boldsymbol{\theta}}_i)$  using a Gibbs sampler initialized at  $\tilde{\mathbf{X}}_i$ .
    Append dataset  $\mathbf{Y}_{i,j}$  to list  $\mathcal{D}$ .
  end for
end for

```

i. For each of the N observations, the sampler cycles through the P full conditional distributions $f(X_p | \mathbf{X}_{-p}, \boldsymbol{\theta})$, which are based on the pseudo-likelihood function, and generates a new value for each variable. This is repeated 100 times for each observation in the sample. Details about the Gibbs sampler implementation can be found in the package – INFORMATION REMOVED FOR BLIND REVIEW –. Any starting state, be it random or observed, yields samples from the same target distribution after sufficient mixing and only affects the rate of convergence of the sampler. The data $\tilde{\mathbf{X}}_i$ are the most plausible under the estimated $\hat{\boldsymbol{\theta}}_i$, and using them as the initial state places the Markov chain in a high-likelihood region under $\hat{\boldsymbol{\theta}}_i$, reducing the burn-in length. On the other hand, a random initialization may place the Markov chain in a low-probability region, requiring a long burn-in phase before reaching the equilibrium. To justify our choice, in Figure X, X and X we present a performance comparison of the starting points. We consider marginal distributions, pairwise distributions, and mixing between the two different initializations for $N = 2,000$, $P = 9$, \mathcal{S} = “random”, $K_{\text{str}} = 10$, and $K_{\text{sample}} = 10$. Furthermore, we set the number of iterations of the Gibbs sampler to 100 and the burn-in (only for the random initial state) to 1,000.

F The global stepsize parameter σ^2

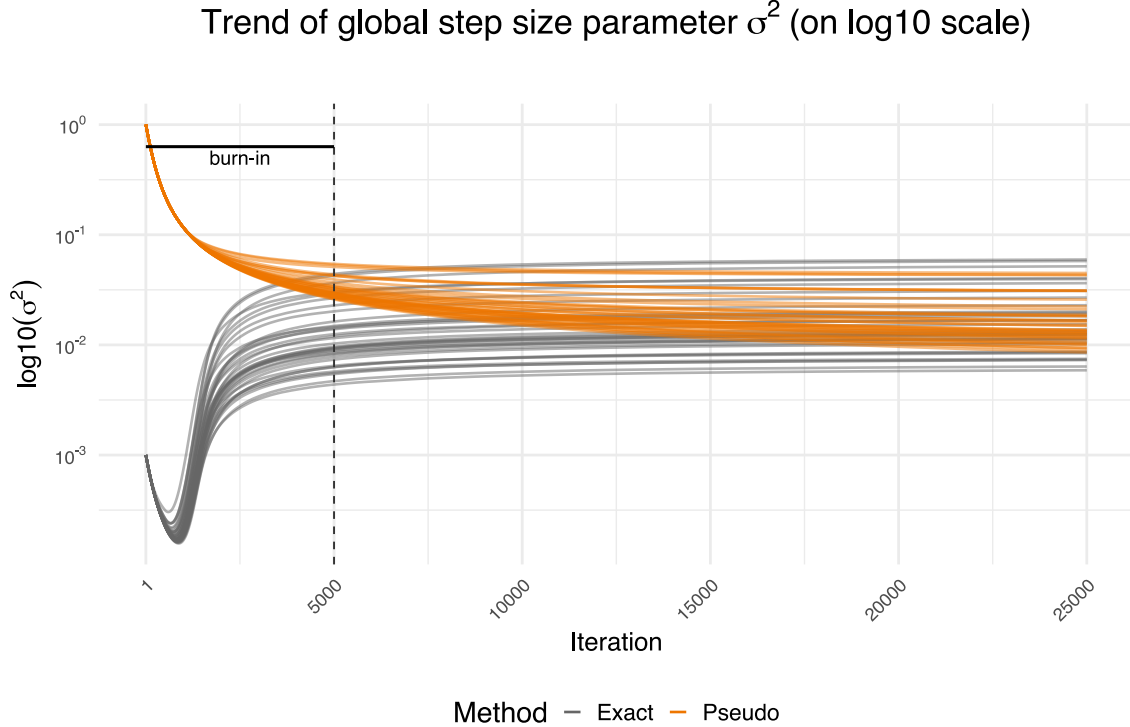


Figure F1: The trend of the global variance parameter σ^2 for the Fisher-MHALA in both the pseudo posterior (represented by orange lines) and in the exact posterior (represented by dark gray lines) for a sample of 5 networks from each of the 36 simulation studies. We initialize the σ^2 parameter at 0.001 in the Fisher-MHALA sampler for the exact posterior, and at 1.0 in the sampler for the pseudo posterior. The parameter is allowed to increase or decrease as illustrated by the figure. For each of the 36 study conditions, the trend is defined by first calculating the cumulative mean of the 5 simulated datasets over 25,000 iterations. We then calculate the mean across the 5 datasets at each iteration. This results in 36 trends for both the exact posterior and the pseudo posterior.

References

Arnold, B. C. and Strauss, D. (1991). Pseudolikelihood estimation: Some examples. *Sankhyā: The Indian Journal of Statistics, Series B (1960-2002)*, 53(2):233–243.

Besag, J. (1974). Spatial interaction and the statistical analysis of lattice systems. *Journal of the Royal Statistical Society Series B: Statistical Methodology*, 36(2):192–225.

Besag, J. (1986). On the statistical analysis of dirty pictures. *Journal of the Royal Statistical Society. Series B (Methodological)*, 48(3):259–302.

Bouranis, L., Friel, N., and Maire, F. (2017). Efficient bayesian inference for exponential random graph models by correcting the pseudo-posterior distribution. *Social Networks*, 50:98–108.

Florez, M., Gottard, A., McAdams, C., Guindani, M., and Vannucci, M. (2025). A bayesian approach for inference on mixed graphical models. *Bayesian Analysis*, 1(1).

Geys, H., Molenberghs, G., and Ryan, L. M. (1997). Pseudo-likelihood inference for clustered binary data. *Communications in Statistics - Theory and Methods*, 26(11):2743–2767.

Godambe, V. P. (1960). An Optimum Property of Regular Maximum Likelihood Estimation. *The Annals of Mathematical Statistics*, 31(4):1208 – 1211.

Haario, H., Saksman, E., and Tamminen, J. (2001). An adaptive metropolis algorithm. *Bernoulli*, 7(2):223.

Heck, D. W. (2018). A caveat on the savage–dickey density ratio: The case of computing bayes factors for regression parameters. *British Journal of Mathematical and Statistical Psychology*, 72(2):316–333.

Hessen, D. J. (2023). Fitting and testing log-linear subpopulation models with known support. *Psychometrika*, 88(3):917–939.

Huber, P. J. (1967). The behavior of maximum likelihood estimates under nonstandard condition. In LeCam, N. and Neyman, J., editors, *Proceedings of the Fifth Berkeley Symposium on Mathematical Statistics and Probability*, Berkeley, CA, USA. University of California Press.

Huth, K. B. S., DeLong, B., Waldorp, L., Marsman, M., and Rhemtulla, M. (2025). Nodewise parameter aggregation for psychometric networks. *Multivariate Behavioral Research*, 60(3):509–517.

Ising, E. (1925). Beitrag zur theorie des ferromagnetismus. *Zeitschrift für Physik*, 31(1):253–258.

Kalichman, S. C. and Rompa, D. (1995). Sexual sensation seeking and sexual compulsivity scales: Validity, and predicting hiv risk behavior. *Journal of Personality Assessment*, 65(3):586–601.

Keetelaar, S., Sekulovski, N., Borsboom, D., and Marsman, M. (2024). Comparing maximum likelihood and maximum pseudolikelihood estimators for the ising model. *advances.in/psychology*, 2.

Kindermann, R. and Snell, J. L. (1980). *Markov Random Fields and Their Applications*. American Mathematical Society.

Lauritzen, S. L. (1996). *Graphical Models*. Oxford University Press.

Lenkoski, A. and Dobra, A. (2011). Computational aspects related to inference in gaussian graphical models with the g-wishart prior. *Journal of Computational and Graphical Statistics*, 20(1):140–157.

Lindsay, B. G. (1988). Composite likelihood methods.

Marsman, M., Huth, K., Waldorp, L. J., and Ntzoufras, I. (2022). Objective bayesian edge screening and structure selection for ising networks. *Psychometrika*, 87(1):47–82.

Marsman, M., van den Bergh, D., and Haslbeck, J. M. B. (2025). Bayesian analysis of the ordinal markov random field. *Psychometrika*, page 1–37.

Miller, J. W. (2021). Asymptotic normality, concentration, and coverage of generalized posteriors. *Journal of Machine Learning Research*, 22(168):1–53.

Mohammadi, A. and Wit, E. C. (2015). Bayesian structure learning in sparse gaussian graphical models. *Bayesian Analysis*, 10(1).

Mohammadi, R., Schoonhoven, M., Vogels, L., and Birbil, S. I. (2025). Scalable bayesian structure learning for gaussian graphical models using marginal pseudo-likelihood. *Bayesian Analysis*, 1(1).

Mulder, J., Wagenmakers, E.-J., and Marsman, M. (2020). A generalization of the savage–dickey density ratio for testing equality and order constrained hypotheses. *The American Statistician*, 76(2):102–109.

Murray, I., Ghahramani, Z., and MacKay, D. (2006). Mcmc for doubly-intractable distributions. In *Proceedings of the 22nd Annual Conference on Uncertainty in Artificial Intelligence (UAI-06)*, pages 359–366. AUAI Press.

Park, J. and Haran, M. (2018). Bayesian inference in the presence of intractable normalizing functions. *Journal of the American Statistical Association*, 113(523):1372–1390.

Pastore, M. and Calcagnì, A. (2019). Measuring distribution similarities between samples: A distribution-free overlapping index. *Frontiers in Psychology*, 10.

Pensar, J., Nyman, H., Niiranen, J., and Corander, J. (2017). Marginal pseudo-likelihood learning of discrete markov network structures. *Bayesian Analysis*, 12(4).

Plummer, M., Best, N., Cowles, K., and Vines, K. (2006). Coda: Convergence diagnosis and output analysis for mcmc. *R News*, 6(1):7–11.

R Core Team (2025). *R: A Language and Environment for Statistical Computing*. R Foundation for Statistical Computing, Vienna, Austria.

Renyi, E. (1959). On random graph. *Publicationes Mathematicae*, 6:290–297.

Robbins, H. and Monro, S. (1951). A Stochastic Approximation Method. *The Annals of Mathematical Statistics*, 22(3):400 – 407.

Schmid, C. S. and Desmarais, B. A. (2017). Exponential random graph models with big networks: Maximum pseudolikelihood estimation and the parametric bootstrap. In *2017 IEEE International Conference on Big Data (Big Data)*, pages 116–121.

Sekulovski, N., Keetelaar, S., Huth, K., Wagenmakers, E.-J., van Bork, R., van den Bergh, D., and Marsman, M. (2024). Testing conditional independence in psychometric networks: An analysis of three bayesian methods. *Multivariate Behavioral Research*, 59(5):913–933.